PHOTOPRODUCTION OF PION PAIRS IN HYDROGEN

Thesis by

Michel A. Bloch

In Partial Fulfillment of the Requirements

For the Degree of

Doctor of Philosophy

California Institute of Technology

Pasadena, California

1958

ACKNOWLEDGMENTS

The author wishes to express his sincere appreciation to Dr. Matthew Sands, his advisor in this work, for his counsel and active assistance in obtaining and analysing the experimental data and for his guidance during the author's graduate residence.

The constant encouragement and continuing interest of Dr. Robert F. Bacher is greatly appreciated. Dr. Robert L. Walker, Dr. Alvin V. Tollestrup, Dr. Ricardo Gomez, Dr. John M. Teem and other members of the staff of the Synchrotron Laboratory have been helpful consultants on numerous occasions.

The author had many valuable discussions with Dr. John Mathews and Dr. Frederik Zachariasen on the theoretical aspect of the experiment.

Dr. Vincent Z. Peterson and Mr. Earle B. Emery are to be thanked for the construction and maintenance of the hydrogen gas target. Mr. Bruce Rule, Mr. Daniel Sell, Mr. Lawrence B. Loucks and others of the engineering staff and crew of the Synchrotron Laboratory have been most helpful during the experiment.

Particular thanks are due to Mr. David D. Elliot and Mr. Sam Berman for their help in the execution and analysis of the experiment.

The partial financial support of the Atomic Energy Commission is gratefully acknowledged.

ABSTRACT

The multiple photoproduction of pions has been observed by detecting, in a magnetic spectrometer, the negative pions which emerged at 60° and at 120° from a high-density hydrogen gas target in the bremsstrahlung beam of the electron synchrotron at the California Institute of Technology. The yields of negative pions "per equivalent quantum" were measured for several values of pion energy and bremsstrahlung cut-off energy. From the variations of the yields with bremsstrahlung cut-off energy, the cross-section for multiple production of pions was obtained. The cross-section shows no large dependence on the angle of emission of the pion from 90° to 150° in the C. M. system. The integral of the cross-section over pion energy is consistent with a constant value $\sigma_{\theta}(\mathrm{CM}) = 4 \times 10^{-30}$ cm^2/ster. for all photon energies between 600 and 1100 Mev. No theoretical prediction is yet available at the photon energies considered in this experiment. The observed dependence of the cross-section on pion energy has been compared to some phenomenological models.

TABLE OF CONTENTS

I. INTRODUCTION

The pion is now believed to be the basic quantum of the nuclear field (1). Attempts to construct theories of the nuclear field in analogy to quantum electrodynamics have met with grave mathematical difficulties because of the large coupling constant of the field. Certain models (2) have given quantitative results for processes involving pions of low energy, but there exists little theoretical framework for the description of events in which pions with kinetic energies above their rest energy can be present. At these higher energies both theory and experiment are complicated by the likelihood that several pions may be involved in any process. This thesis is concerned with the production of two or more mesons from the interaction of high energy photons with the proton.

The interaction of a high-energy photon with a proton can yield pions via several processes:

$$\gamma + P \longrightarrow N + \pi^{+}$$

$$\longrightarrow P + \pi^{o}$$

$$\longrightarrow P + \pi^{+} + \pi^{-}$$

$$\longrightarrow P + \pi^{o} + \pi^{o}$$

$$\longrightarrow N + \pi^{+} + \pi^{o}$$

$$\longrightarrow P + \pi^{+} + \pi^{-} + \pi^{o}$$ etc. (if enough energy is available).

Because of charge conservation, negative pions cannot be obtained in a single pion photoproduction in hydrogen. A negative pion

indicates a pair production, $\gamma + P \longrightarrow P + \pi^+ + \pi^-$, or a reaction of higher multiplicity (up to five pions can be produced with a 1 Gev* photon).

The photoproduction of pion pairs was first observed at the California Institute of Technology using a 500 Mev bremsstrahlung beam. Peterson and Henry (3) used nuclear emulsions as detectors and Sands, Bloch, Teasdale and Walker (4) detected the negative pions with a magnetic spectrometer. More recent results on the continued scanning of plates from exposures taken with 500 Mev bremsstrahlung have been published by Peterson (5). These experiments showed the existence of the process and gave a π^-/π^+ ratio at 73° of about 0.02 for 50 Mev pions and about 0.15 for 15 Mev pions.

More extensive results were obtained at Stanford University. Friedman and Crowe (6) measured the yields of negative pions and their energy spectra at laboratory angles of 60° and 75° and for several bremsstrahlung energies up to 600 Mev. The main features of their results are:

(1) a slow initial rise in the excitation function (76 Mev pions);

(2) at maximum photon energies up to 600 Mev, the energy spectrum of the negative pions is peaked at low energies. Their results are in fair agreement with the theoretical predictions of Cutkosky and Zachariasen (7). The yield per effective photon** at 600 Mev is

---

* The international convention is used: 1 Gev = 10^9 ev.

** This quantity is defined in Part IV, Section C.

equal to 6×10^{-33} cm^2/Mev-ster for 76 Mev negative pions emitted at 60^o. An increase in the yield of positive pions for bremsstrahlung cut-off energies above the threshold for pair production is attributed to the contribution of (π^+, π^-) and (π^+, π^o) pairs.

An experiment on the photoproduction of pion multiplets is in progress at Cornell University. Woodward, Wilson and Luckey (8) detect 40 Mev negative pions produced in a liquid hydrogen target at a laboratory angle of 35^o by x-rays of the Cornell synchrotron. They observe a rapid increase in the negative pion yield at maximum bremsstrahlung energies between 600 and 700 Mev, then the yield becomes practically constant up to 1 Gev.

A report on the preliminary results of the experiment described in this thesis has been made at the Boulder Meeting of the American Physical Society (9).

Additional information on the state with a nucleon and two or more mesons has been obtained at Brookhaven by using the π^- beam produced in the Cosmotron. Collisions of these mesons with protons have been observed in a hydrogen diffusion cloud-chamber and in nuclear emulsions (10-12). The results are said to be indicative of decay of an excited pion-nucleon system in the resonant (3/2, 3/2) state.

The knowledge of the energy and direction of the negative pion alone, in a multiple photoproduction, is not sufficient to determine the energy of the incident photon because there are at least three particles in the final state of the system. The photons, on the other hand, are obtained in a synchrotron through bremsstrahlung of high energy

electrons and have a continuous energy spectrum. Negative pions selected at a given angle and energy can be produced by all the photons present in the bremsstrahlung with energies greater than a threshold which depends on the pion energy and angle. It is not possible, then, to determine from a single measurement a cross-section for the photoproduction of pion multiplets. Each experimental point gives a yield which is an integral of the cross-section over photon energy.

By subtracting the experimental yields obtained at two different bremsstrahlung energies E_1 and E_2, the contribution to the yields due to photons in the range of energies between E_1 and E_2 can be isolated. The cross-section for a photon energy in the neighborhood of $1/2\ (E_1 + E_2)$ can then be given for a photon energy resolution width of about $E_2 - E_1$. Such an analysis is, of course, possible on the experiments described above but the statistical errors on the yields are so large as to make the differences quite inaccurate.

In this work, negative pions produced in hydrogen by the x-ray beam of the Caltech electron synchrotron are detected by a specially designed magnetic spectrometer. Its large solid angle of acceptance (about 0.02 steradian) and momentum resolution of about 16 °/o made possible the high counting rate necessary for the desired accuracy in the yields.

An investigation of the multiple production of pions for bremsstrahlung cut-off energies up to 1.10 Gev was performed at two laboratory angles (60° and 120°) and for pion kinetic energies of 50, 100, and 150 Mev. The yields were obtained with sufficient precision to make an

evaluation of the cross-sections meaningful when differences between yields are taken. By changing the polarity of the magnet, positive pions were detected. A check on the experimental parameters was then possible by comparison with the earlier results for single pion photoproduction. Variation of the positive pion yield with bremsstrahlung cut-off energy gave some indications on the (π^+, π^-) and (π^+, π^o) pair processes.

II. EXPERIMENTAL ARRANGEMENT

A. Experimental Layout

A general plan view of the experimental equipment is shown in figure 1. The x-ray beam is first collimated by a tapered lead primary collimator 1.8 cm. in diameter located in one of the magnet legs of the synchrotron. One and one-half meters from the primary collimator, the beam passes through an opening in a lead wall, 10 cm. thick, which is located about 2 meters from the target and serves to shield the apparatus from stray radiation. Before striking the gas target, the beam passes through a 10 cm. thick lead scraper, 4.5 cm. in diameter which cleans up the edges of the beam without introducing further collimation. The cylindrical gas target has an inner diameter of about 5 cm. (2 in.), is 43 cm. long and is aligned in such a way that the beam does not touch its side walls. About 2 meters behind the gas target, the beam passes through a secondary lead collimator, between the poles of several permanent magnets and through a liquid hydrogen target associated with other experiments. Finally it impinges on a thick-walled copper ionization chamber located in a large lead block.

The pions produced in the hydrogen gas are deflected by an analysing magnet and detected in a counter telescope which is enclosed in a lead house having walls 10 cm. thick on the side and back of the telescope, 5 cm. on the top.

B. The Gas Target

Hydrogen gas at a pressure of about 150 atmospheres and at a temperature of about $100^{\circ}K$ is enclosed in a thin-walled vessel. This

Figure 1. General Plan View of the Experimental Equipment.

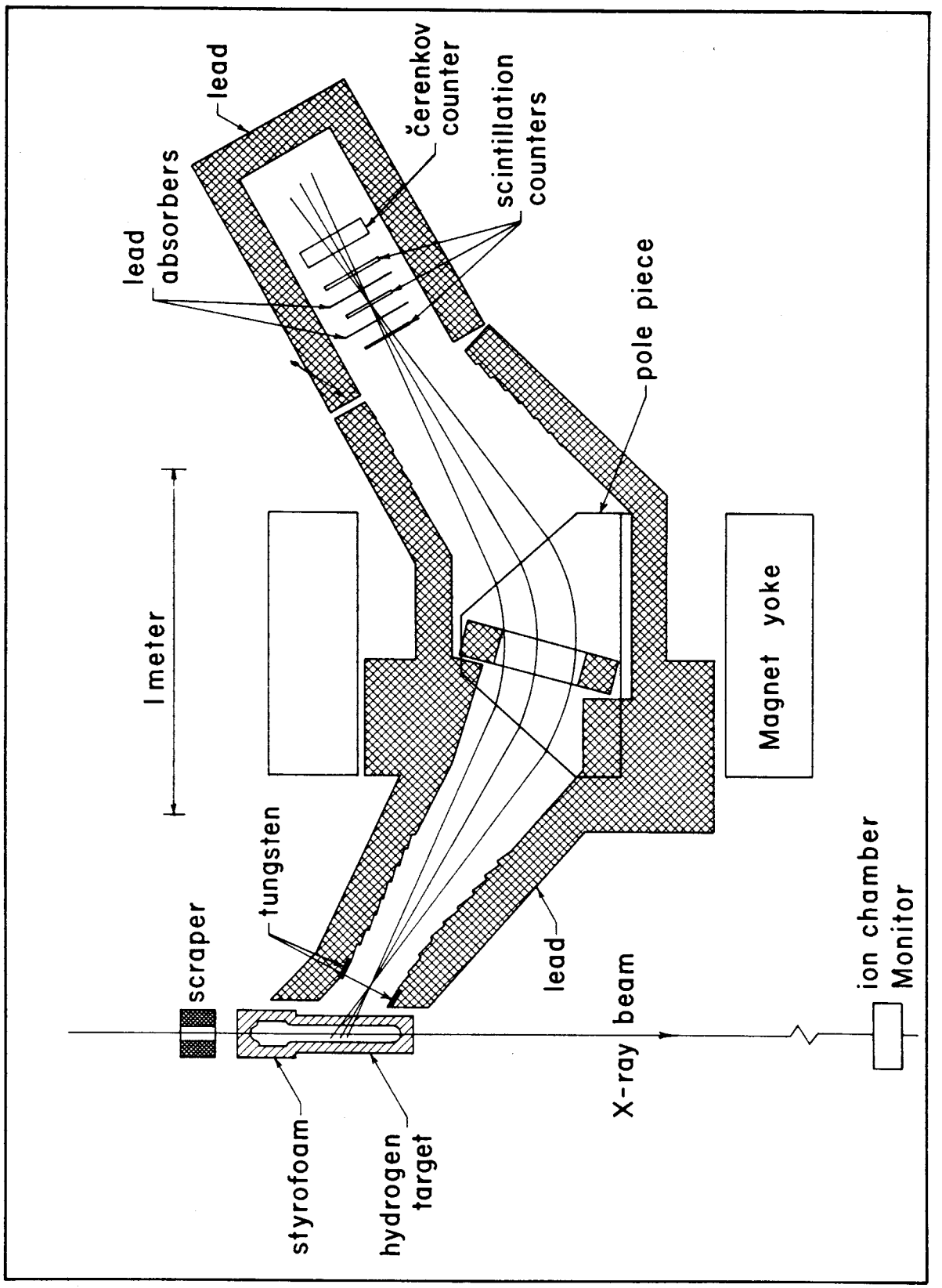
lead
absorbers
lead
čerenkov
counter
scintillation
counters
pole piece
1 meter
Magnet yoke
tungsten
scraper
lead
X-ray beam
ion chamber
Monitor
styrofoam
hydrogen
target

vessel has a cylindrical shape 43 cm. long with 5 cm. inner diameter and has 0.075 cm. thick steel walls. It is cooled by contact with a liquid nitrogen reservoir and is surrounded by 4 cm. of Styrofoam* insulation (see figure 2).

The counting rate of negative pions will be directly proportional to the number of protons interacting with the x-ray beam hence to the density of the hydrogen in the target. In the reduction of the data, the cross-sections will be obtained from differences between the pion yields at two different bremsstrahlung energies. Even though the error introduced in the yields by uncertainties in the determination of the density may not be too important, the corresponding relative error in the cross-sections can be much larger if the differences are small compared to the yields. Care should be taken therefore, to measure the hydrogen density (along with the other experimental parameters) as accurately as possible in so far as variations from run to run are concerned.

The density is found from temperature and pressure measurements by interpolation from data of Johnston et al (13). The pressure of the hydrogen in the target is measured with a Bourdon gauge, the error in reading being about 0.5 $^{o}/o$. The temperature of the hydrogen is measured by means of two iron-constantan thermocouples, one at the tip of the target and the other one in a position on the target close to the liquid nitrogen reservoir. A reference temperature is provided by a

---

* Registered trade mark of the Dow Chemical Company: expanded polystyrene, density 0.025 g/cm^3.

Figure 2. The Hydrogen Gas Target

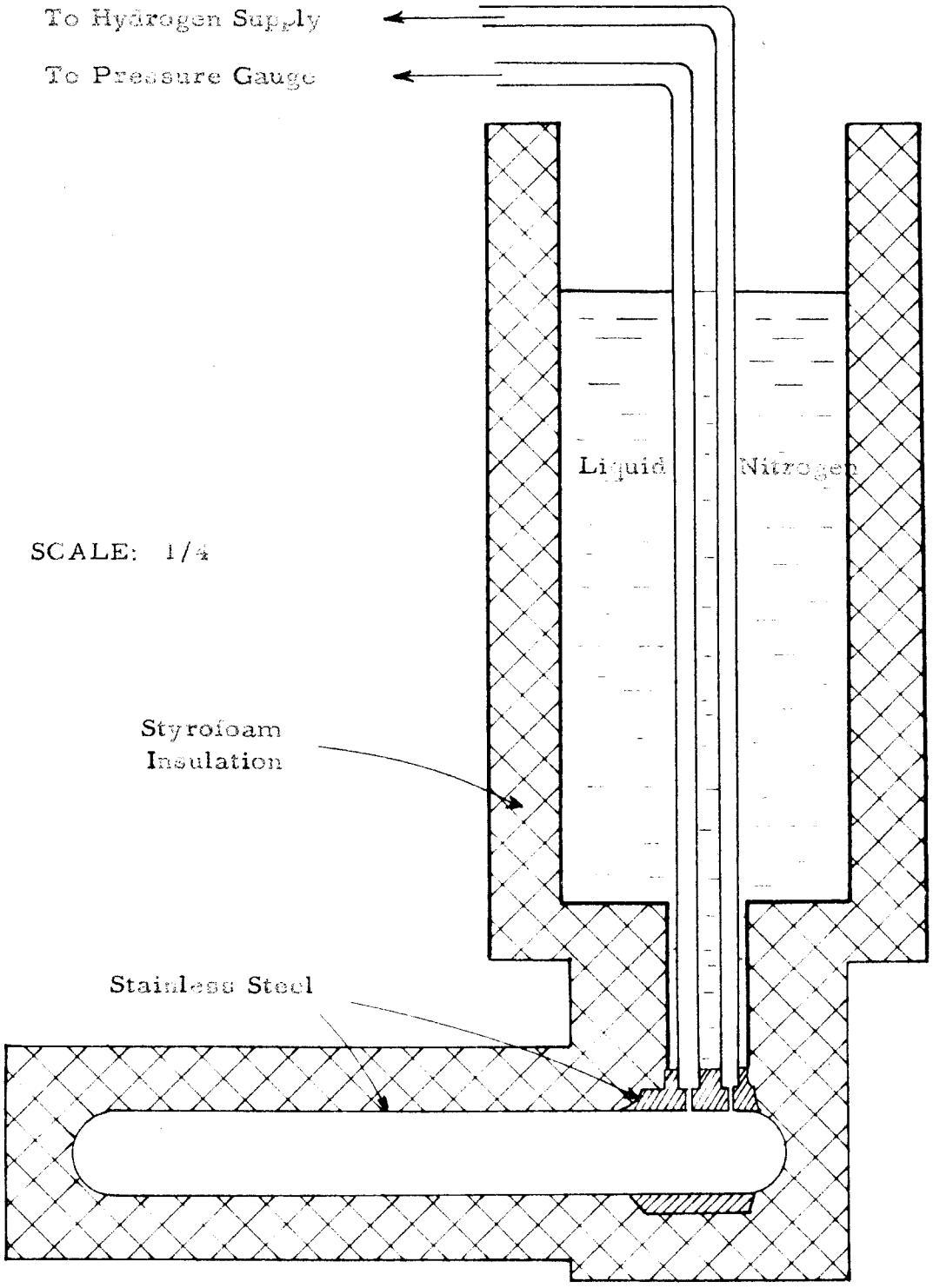
To Hydrogen Supply
To Pressure Gauge
Liquid Nitrogen
SCALE: 1/4
Styrofoam Insulation
Stainless Steel

third thermocouple immersed in liquid nitrogen. The temperature of the hydrogen is assumed to be the average between tip and base temperatures and can be measured to about 0.5°K accuracy. A typical value of the density is 0.030. The absolute error in the density measurements was about 3 °/o, the relative error from run to run was about 1 °/o.

The hydrogen used in the experiment was analysed with a mass spectrograph (14) with the following results in molecular percentages:

Hydrogen:	99.90
Nitrogen:	0.06
Oxygen:	0.04
Other:	less than 0.005.

C. The Analysing Magnet

The particles emitted from the target are selected in momentum and direction by a uniform field symmetrical wedge magnet. For the central trajectory, the angle of deflection is 60°, the total length of the trajectory between foci is 230 cm.

Negative pions are produced in abundance in the steel ends of the bomb. A set of defining slits permit only those pions produced in the gas to enter the magnet deflecting system. One defining aperture is placed at one of the focal point of the spectrometer and consists of two lead bricks placed 15.2 cm. (6 in.) apart in a line perpendicular to the central focused trajectory. Each brick has a tungsten plate 1.25 cm. thick, 5 cm. wide and 6.3 cm. high embedded in it. Another aperture is placed between the pole pieces of the magnet. Its horizontal

dimension (25.4 cm.) is designed to restrict the trajectories to a region of uniform field (apart from the entrance and exit edges of the magnet). Its vertical size and position are determined from the condition of having as large a solid angle as possible and preventing the detection of particles scattered on the pole pieces. Additional lead shielding is placed so as to reduce a background of charged particles produced in the air and in the synchrotron and shielding material. Figure 3 shows horizontal and vertical projections of the central and limiting trajectories.

For the focal points chosen, the focused particles trajectories have a radius of curvature of 61 cm. in the uniform field. The solid angle of acceptance at the focal point is about 0.02 steradian and the momentum resolution dp/p is 16 ^{o}/o for a counter width of 15.2 cm. (6 in.). The position of the foci and other magnet characteristics were checked by the stretched wire method. The design of the spectrometer and experimental test of the magnet are described in a separate report (15).

Magnetic fields up to 14 kilogauss are obtained when the magnet is energized from a 30 KW d-c generator. The magnetic field intensity was measured for several magnet currents with a nuclear-resonance magnetometer designed by Donoho (16), the generator was operated with a current regulator which held the current constant to better than 0.5 ^{o}/o during a run. Figure 4 shows directly the analysed pion momentum as a function of the current in the coils.

Figure 3a. Horizontal Projections of the Trajectories in the Spectrometer.

Figure 3b. Limiting Trajectories in the Vertical Direction.

The trajectories shown here have their horizontal projections along the central ray. The distance between foci and the length of the trajectories inside the magnetic field vary when the trajectories are displaced toward the apex of the magnet or away from it. A slight vertical defocusing was taken into account in the design of the lead aperture but is too small to be indicated in the figure.

a)

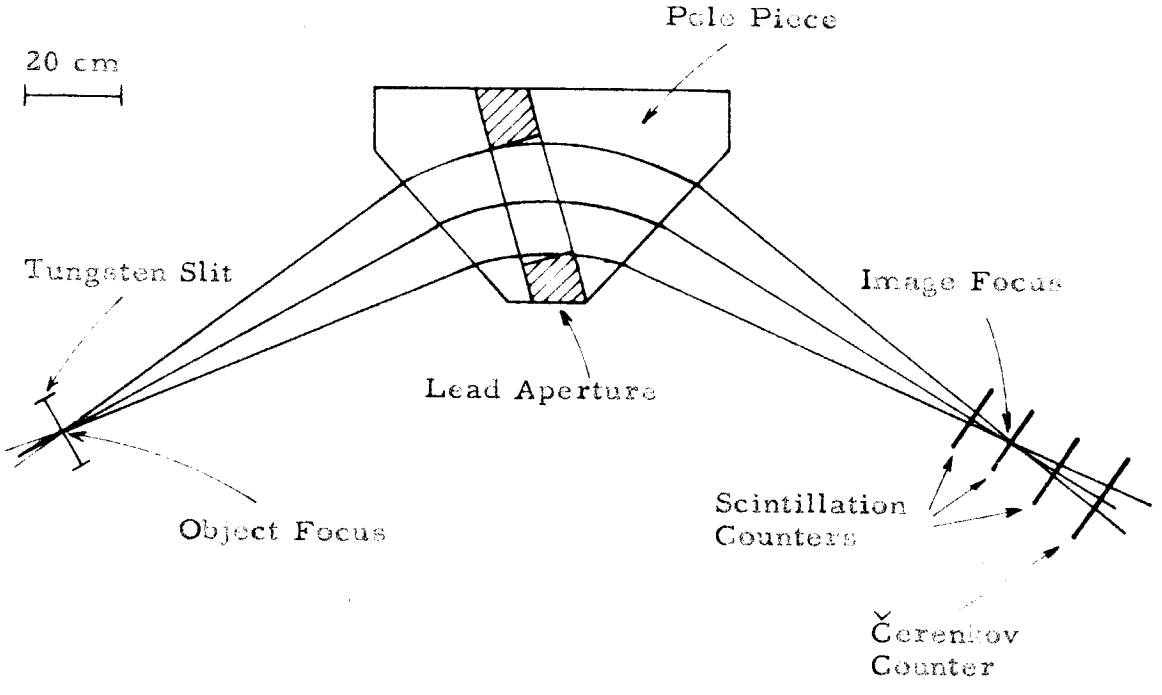
20 cm
Pole Piece
Tungsten Slit
Image Focus
Lead Aperture
Object Focus
Scintillation
Counters
Čerenkov
Counter

b)

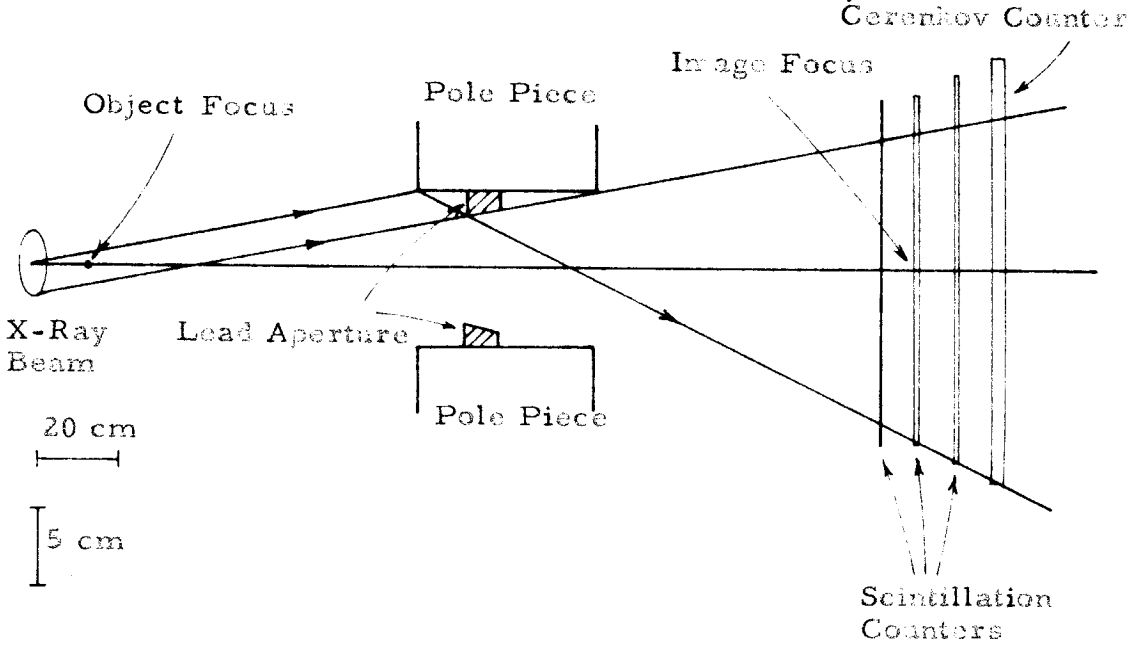
Čerenkov Counter
Image Focus
Object Focus
Pole Piece
X-Ray
Beam
Lead Aperture
Pole Piece
20 cm
5 cm
Scintillation
Counters

Figure 4. Pion Momentum Versus Current in the Magnet Coils.

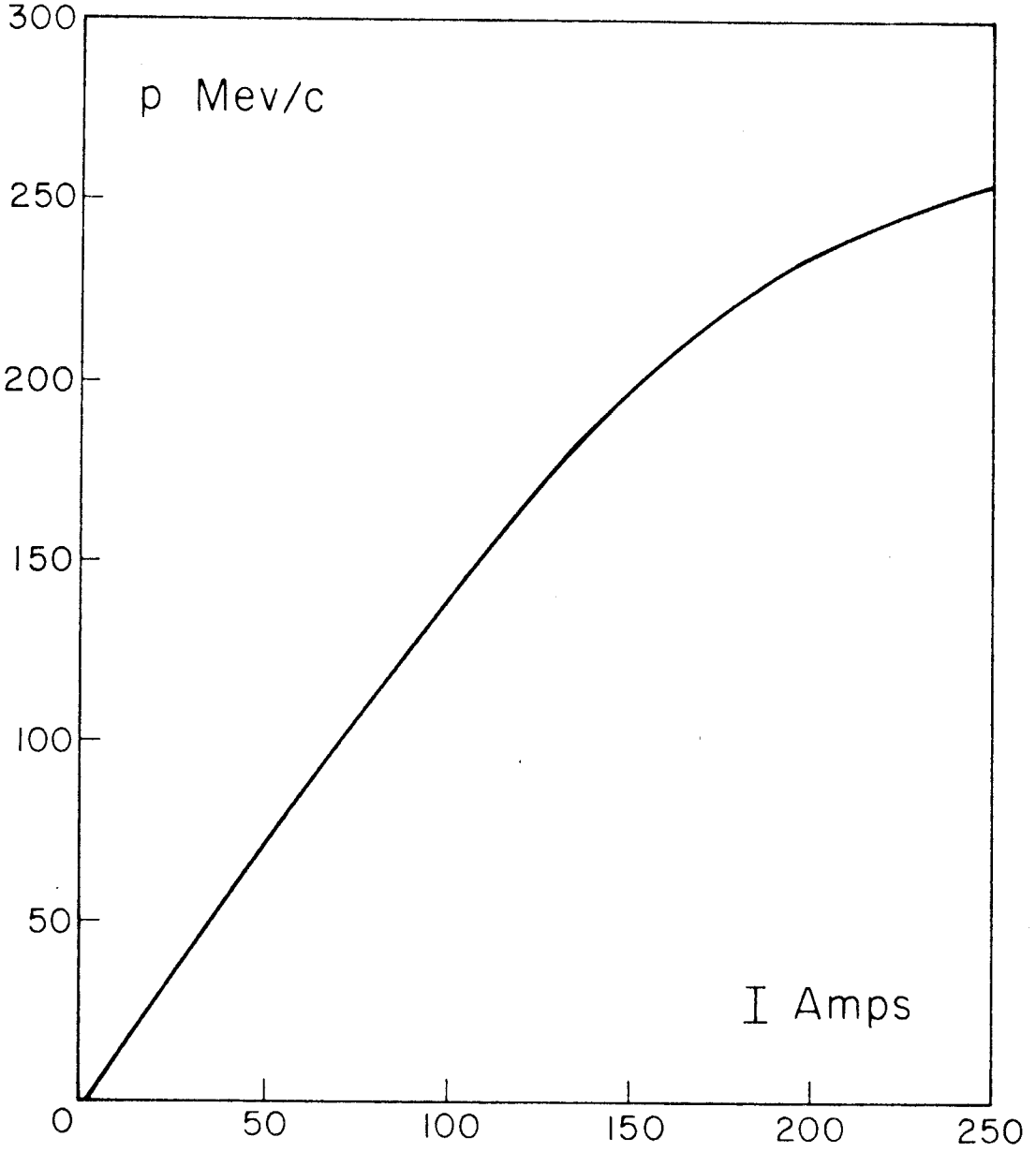
300
p Mev/c
250
200
150
100
50
0
50
100
150
200
250
I Amps

D. The Counter Telescope

The particles selected by the magnet are registered by a counter telescope located at the second focal point. The telescope consists of three scintillation counters and one Čerenkov counter. The plastic scintillation cells have dimensions 0.635 x 15.2 x 22.8 cm., 1.27 x 15.2 x 22.8 cm., 1.27 x 17.8 x 25.4 cm. (1/4 x 6 x 9 in., 1/2 x 6 x 9 in., 1/2 x 7 x 10 in.) respectively and each are viewed by two ten-stage photomultipliers. In two counters RCA 5819's are used, the other one is equiped with Dumont 6292's. The Čerenkov counter is made of lucite, 5.08 cm. thick, by 20.3 cm. by 27.9 cm. (2 x 8 x 11 in.) (discounting tapered extensions about 10 cm. long to connect the photo-multipliers to the main body of the counter). Two photomultipliers (Dumont 6363's; 3 in. photocathode) are used in this counter which is placed in last position in the telescope. Mu-metal shields provide magnetic shielding on all the phototubes.

The counters are clamped vertically to a steel frame, their position along this frame being adjustable. In practice, they were kept as close to each other as possible (about 10 cm. between consecutive counters). Absorbers can be placed between the counters and it was found necessary to place 0.3 cm. lead absorber between the first and second counter and between the second and third in order to reduce background coincidences.

E. Beam Monitoring

The energy of the electrons accelerated in the synchrotron is kept constant for a 20 msec. time-interval during which they strike an

internal radiator and produce a bremsstrahlung beam. The total energy in the beam is measured by integrating the current from an ionization chamber with 2.5 cm. thick copper walls of the type developed at Cornell University. The charge collected from this chamber is proportional to the total energy in the beam for a given maximum bremsstrahlung energy, the proportionality constant varying slowly with the maximum energy. The proportionality constant was calibrated with a "Quantameter" of the type developed by Wilson (17). It is customary in this laboratory to normalize the data to a standard beam monitor reading called BIP (beam integrator pulse). Gomez (18) found that 1 bip = 0.99×10^{12} Mev at a maximum bremsstrahlung energy of 497 Mev. The dependence of the bip on bremsstrahlung cut-off energy is given in figure 5a.

Since there was a secondary collimator behind the gas target, the total beam energy indicated by the beam monitor used in the experiment was less than the energy in the beam striking the target. This correction was obtained by comparing the reading of the thick ionization chamber when placed in front of the secondary collimator and in its normal position, a thin ionization chamber in front of the gas target being used as a monitor for both runs. A dependence on the maximum photon energy was found, due to a change in the radial distribution of photons in the beam. Figure 5b shows the ratio of energy in the beam striking the target to the energy detected in the beam monitor as a function of the bremsstrahlung cut-off energy.

Figure 5a. Energy Flux in the Beam for 1 "bip" as a Function of the Bremsstrahlung Cut-Off Energy.

Figure 5b. Ratio of the Beam Energy Flux Striking the Target to the Beam Energy Flux Detected by the Monitor as a Function of the Bremsstrahlung Cut-Off Energy.

a)

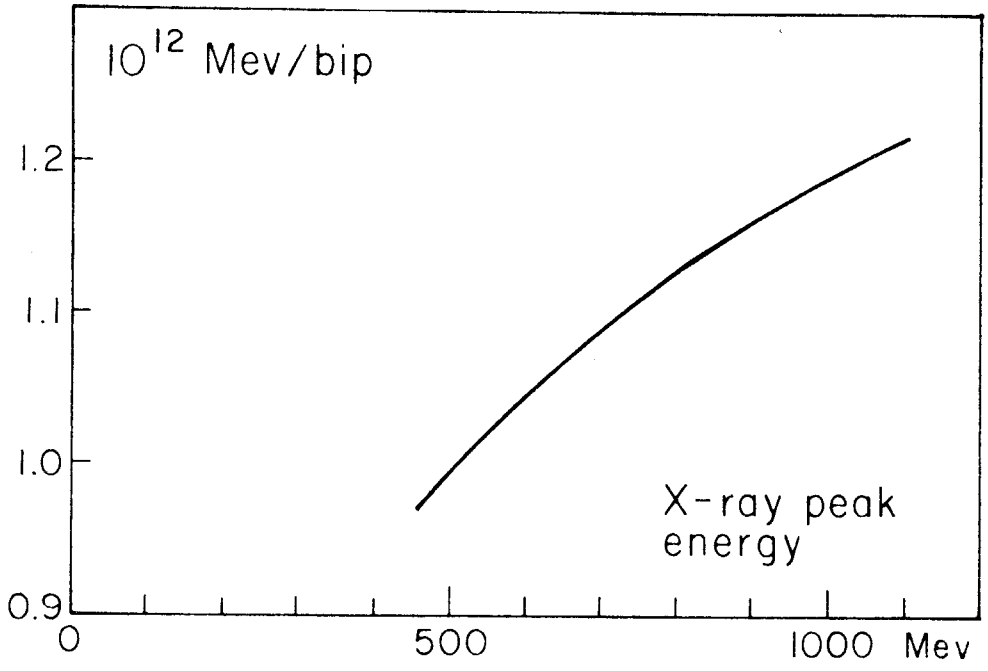
10^{12} Mev/bip
1.2
1.1
1.0
0.9
X-ray peak energy
0
500
1000 Mev

b)

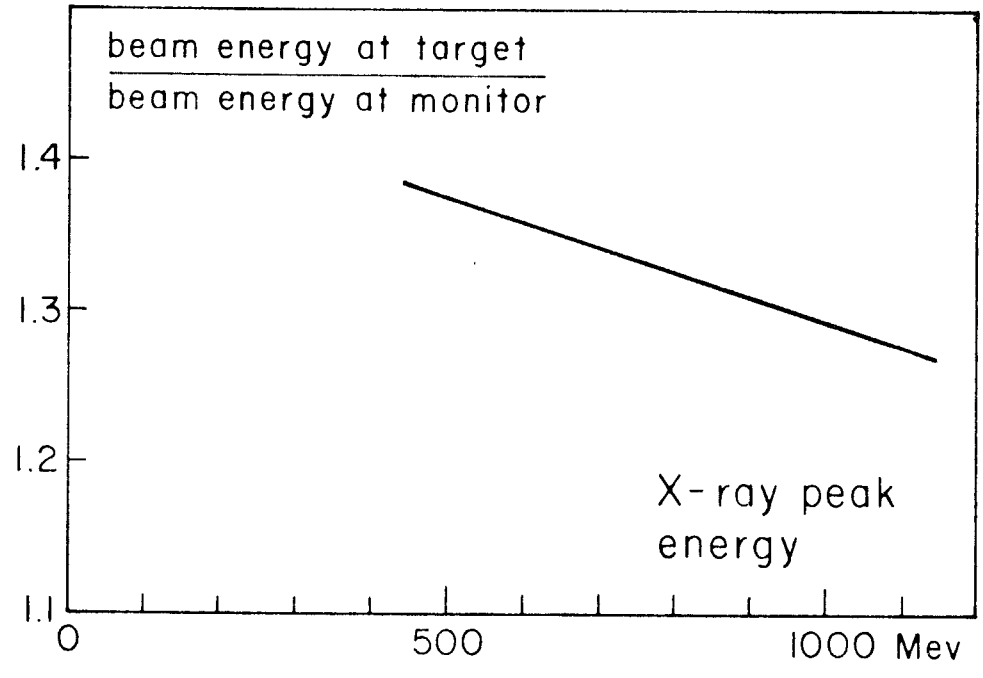
beam energy at target
beam energy at monitor
1.4
1.3
1.2
1.1
X-ray peak energy
0
500
1000 Mev

When attempting to obtain cross-sections by differences between the negative pion yields at different bremsstrahlung energies, the shape of the bremsstrahlung spectrum has to be known to determine the photon energy resolution function. The bremsstrahlung spectrum has been measured by Donoho, Emery and Walker (19) using a pair spectrometer. Let $B(E_o, k/E_o)dk/k$ be the number of photons of energy k (within dk) in a bremsstrahlung beam having E_o as maximum photon energy, and having a total energy also equal to E_o. That is, $B(E_o, k/E_o)$ is defined such that:

$$\int_0^{E_o} B(E_o, k/E_o)dk = E_o \ .$$

$B(E_o, k/E_o)$ is plotted in figure 6 as a function of k/E_o. The area under the curve is unity. The spectrum shape has been found identical for E_o = 700 and 1000 Mev. Within the experimental errors it drops abruptly at $k = E_o$ as indicated in figure 6.

F. Electronics

Figure 7 is a block diagram of the electronics used in this experiment. The anodes of the two photomultipliers of each counter are connected in parallel. The outputs of the scintillation counters are first preamplified close to the telescope. The preamplifier Model 25 has delay-line clipping and gives pulses of about 0.5 μsec. duration The signals from the preamplifiers are led to Model 522A amplifiers in the counting area by about 25 meter length of coaxial cable. The

Figure 6. Bremsstrahlung Spectrum.

Measurement at E_o = 700 Mev and E_o = 1000 Mev gave identical results.

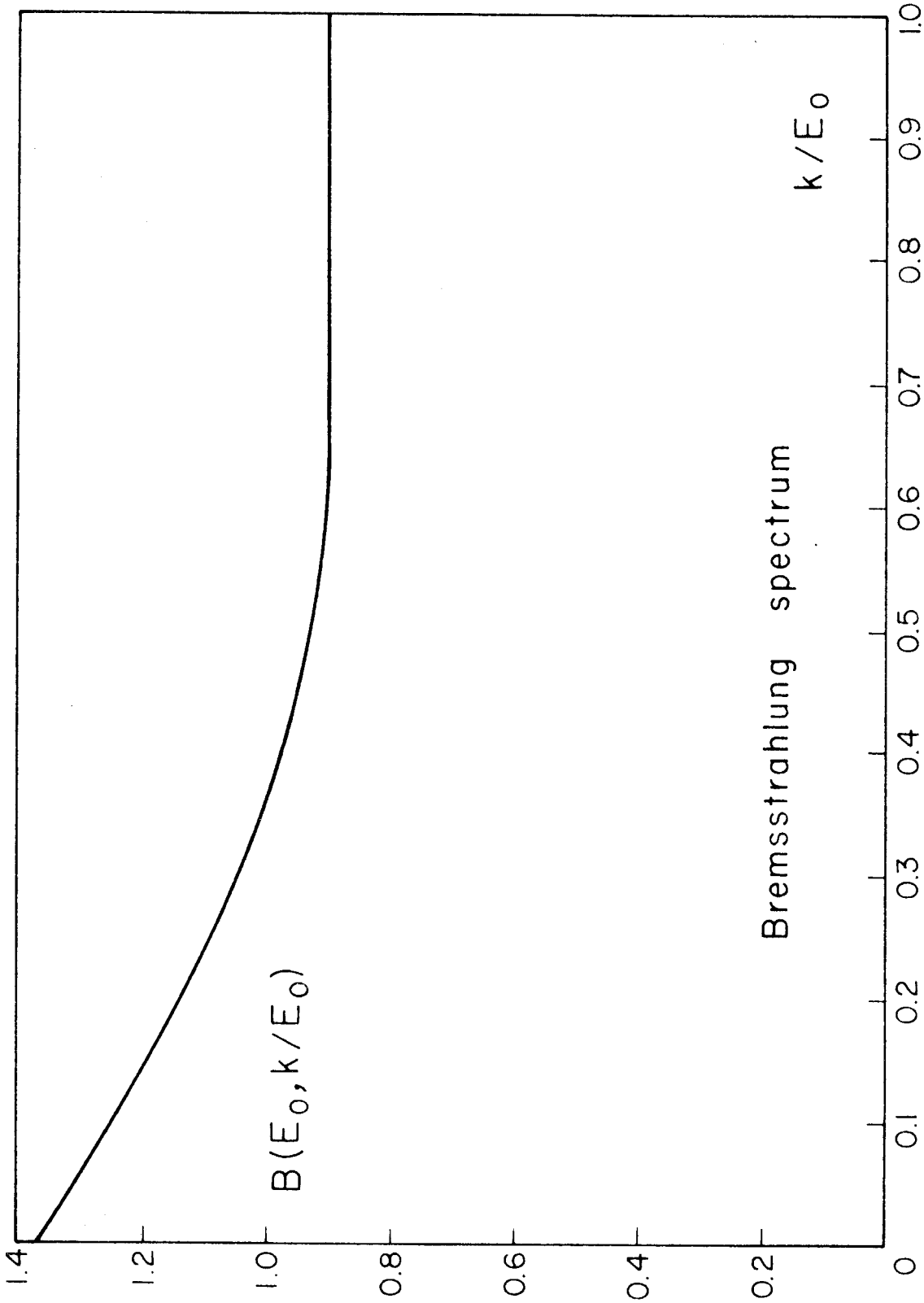
Bremsstrahlung spectrum
$B(E_0, k/E_0)$
k/E_0
0
0.1
0.2
0.3
0.4
0.5
0.6
0.7
0.8
0.9
1.0
0.2
0.4
0.6
0.8
1.0
1.2
1.4

Figure 7. Electronics Block-Diagram

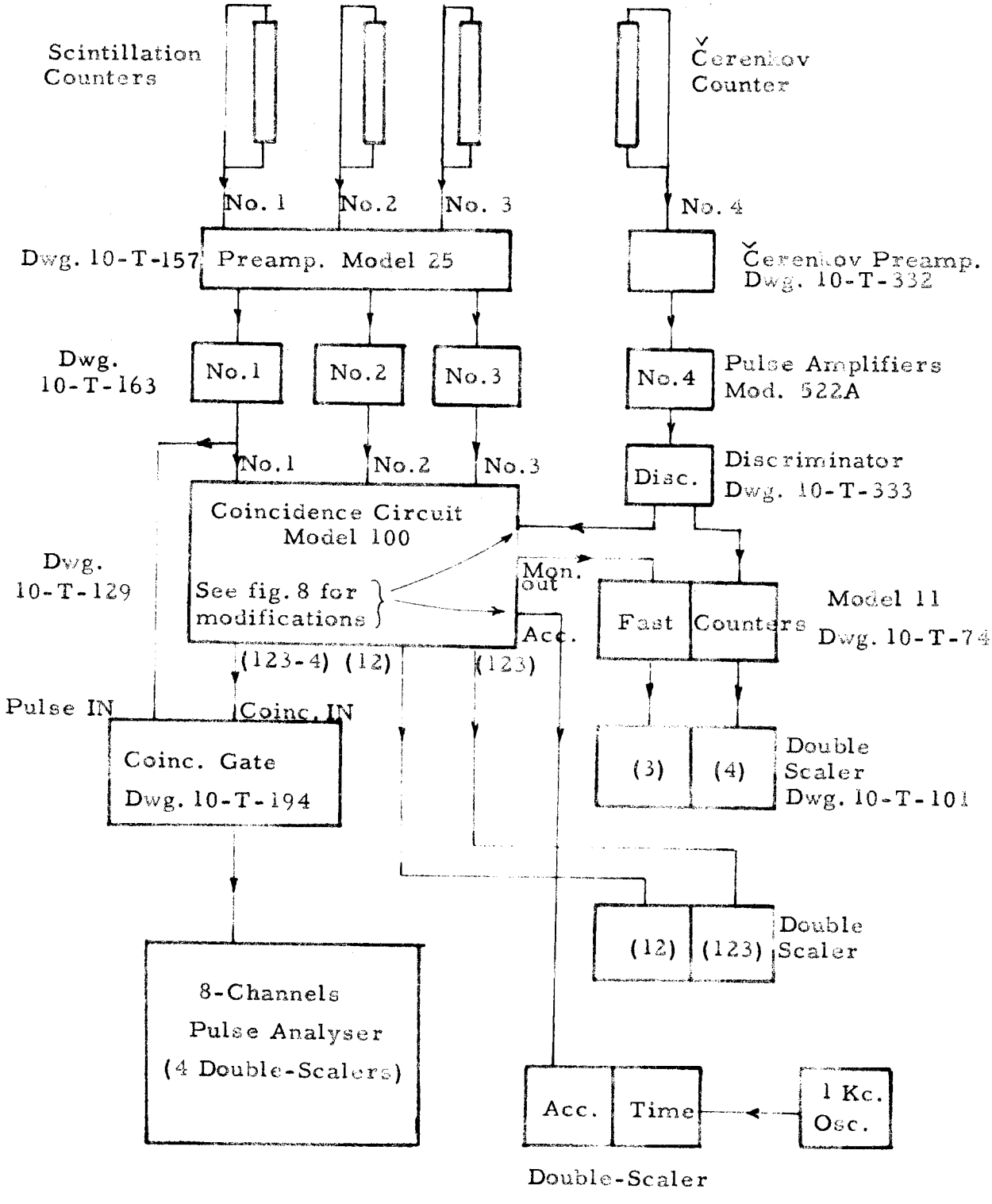
Scintillation Counters
Čerenkov Counter
No. 1
No. 2
No. 3
No. 4
Dwg. 10-T-157
Preamp. Model 25
Čerenkov Preamp. Dwg. 10-T-332
Dwg. 10-T-163
No. 1
No. 2
No. 3
No. 4
Pulse Amplifiers Mod. 522A
No. 1
No. 2
No. 3
Disc.
Discriminator Dwg. 10-T-333
Coincidence Circuit Model 100
Dwg. 10-T-129
See fig. 8 for modifications
Mon. out
Acc.
Fast Counters
Model 11 Dwg. 10-T-74
(123-4)
(12)
(123)
Pulse IN
Coinc. IN
Coinc. Gate Dwg. 10-T-194
(3)
(4)
Double Scaler Dwg. 10-T-101
(12)
(123)
Double Scaler
8-Channels Pulse Analyser (4 Double-Scalers)
Acc.
Time
1 Kc. Osc.
Double-Scaler

amplifiers have a rise time of 0.07 μsec. and a maximum gain of 2,500.

A special preamplifier was designed for the Čerenkov counter to accomodate the small pulses arising from Čerenkov light. It has a gain of about 30 with a rise time of 0.07 μsec.

A coincidence circuit Model 100 was used, slightly modified so that triggers from an event which gives triple coincidence in the scintillation counter and no signal in the Čerenkov counter, (123-4), can be obtained (see figure 8a). The resolving time of this circuit is 0.28 ∓ 0.02 μsec. for triple coincidences and 0.5 μsec. for anti-coincidence. Chance coincidences are monitored by delaying by 2.5 μsec. the coincidences between pulses from the two first counters, and counting their coincidences with pulses from the third counter, (see figure 8b for the corresponding modification in the coincidence circuit Model 100).

A gating circuit passes the pulse from one amplifier whenever a selected coincidence signal is received from the coincidence circuit. This pulse is then analysed in an eight-channel pulse-height analyser. The pulse spectrum from the analyser provides further identification of a particle through its energy loss in the counter.

The number of single pulses from one of the scintillation counters and from the Čerenkov counter are monitored by fast scalers followed by a decimal scaler. All scalers are turned on only during the beam pulse of the synchrotron by a "beam gate" pulse (about 40 msec duration). The total ON-time of each run was determined by counting in one scaler pulses from a 1 KC oscillator.

Figure 8a. Modification of the Model 100 Coincidence Circuit in Order to Obtain (123-4) Triggers.

The complete circuit is shown on Dwg. 10-T-129.

Figure 8b. Modification of the Model 100 Coincidence Circuit in Order to Monitor Chance-Coincidences.

The chance-coincidence pulses are obtained at the old (1.3) outlet.

a)

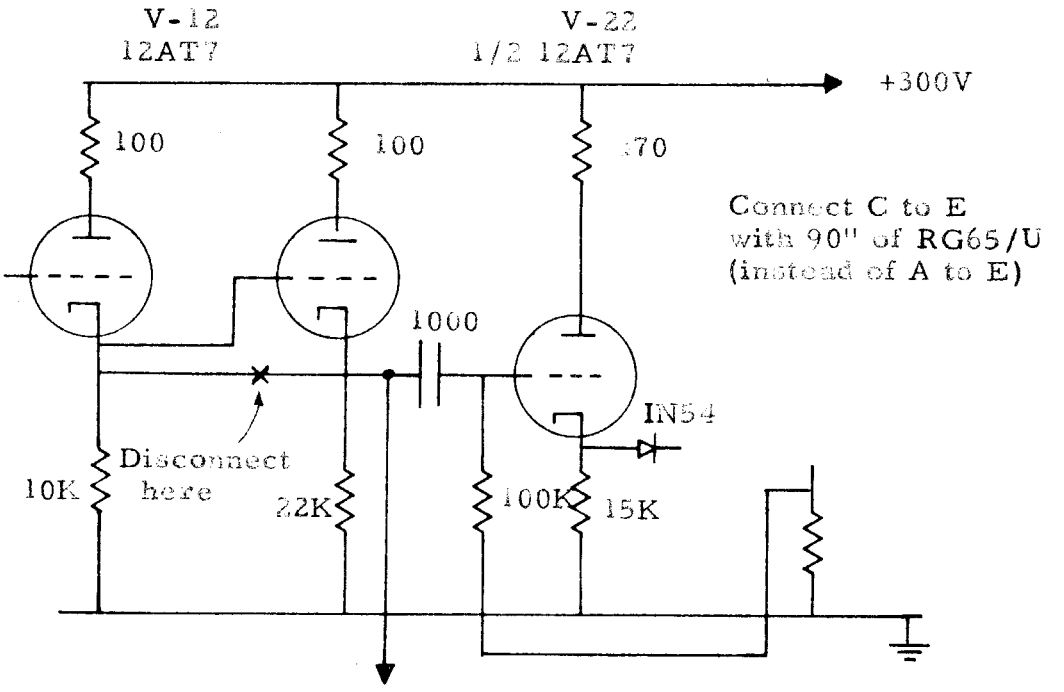

To Discriminator No.

b)

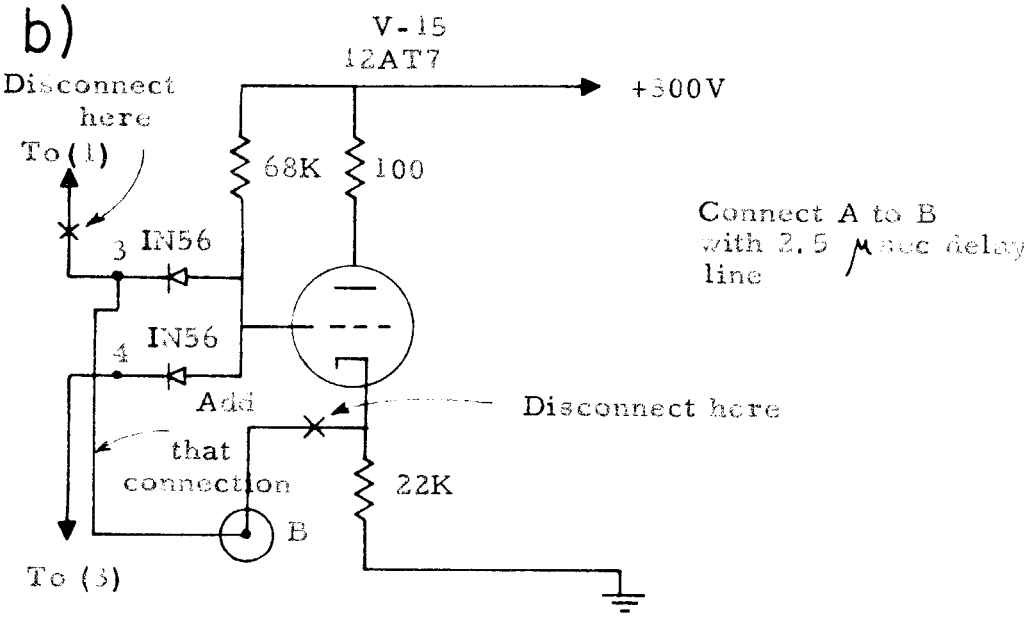

III. EXPERIMENTAL PROCEDURE

A. Alignment of the Equipment

The first step in the experiment was to align the target with the x-ray beam from the synchrotron. An x-ray picture of the target walls was obtained with the uncollimated beam and the alignment was checked by taking a picture of the collimated beam on the same plate. When a satisfactory alignment of the beam and the target was achieved, the lead scraper which is mounted rigidly with respect to the bomb is then aligned along the beam. The magnet, the tungsten slit, lead bridges and counters are placed according to a lay-out drawing, special care being taken to shield the spectrometer against particles produced at the ends of the bomb. A final test of the alignment and shielding arrangement is obtained when background runs are made with an empty target. In all cases the background counting rate was small compared to the one obtained with hydrogen in the target.

B. Pion Identification

The magnet selects particles of given momentum and charge. A further discrimination has to be performed to separate the selected particles into electrons, protons and pions.

The polarity of the magnet was first set to focus positive particles. For the momenta selected by the magnet, protons have too short a range to give the required triple coincidences so the particles detected by the counter telescope were positive pions and positrons. At the angles considered in this experiment, the positive pions were

much more numerous than the positrons and a practically pure beam of mesons crossed the counters.

The high voltage on each of the two phototubes in a counter was adjusted to give signals of approximately equal amplitudes. Then the gain in each amplifier was set in such a way that the counting efficiency for a meson crossing the counter was about 100 ^{o}/o when the biases of the discriminators in the coincidence circuit were set at 20 volts. In other words, the probability that the signal from the pion was less than 20 volts should be small. This was checked by analysing the pulse height from each counter when a triple coincidence was obtained. A typical pulse height spectrum for π^{+} is shown in figure 9a.

It was found from pulse analysis of negative pions from carbon that the gains of the phototubes vary less than 5 ^{o}/o when the polarity of the magnet is reversed. The detecting efficiency is then the same for positive and negative pions.

The number of negative pions and electrons emitted from a hydrogen target are of the same order of magnitude. Discrimination against electrons can be achieved using the pulse height spectrum if the mesons lose appreciably more energy in the counter than the electrons (which are minimum ionizing). Since the resolution of the counters is about 35 ^{o}/o a good separation of the meson and electron peaks can be obtained only for low-energy mesons. For example, a 50 Mev meson gives a signal 1.6 times minimum and its discrimination against electrons is still possible. Figure 9b gives the pulse spectrum for a mixture of electrons and pions when the energy of the

Figure 9a. Typical Pulse-Height Spectrum for 50 Mev Positive Pions.

Figure 9b. Pulse-Height Spectrum for a Mixture of 50 Mev Negative Pions and Electrons.

a)

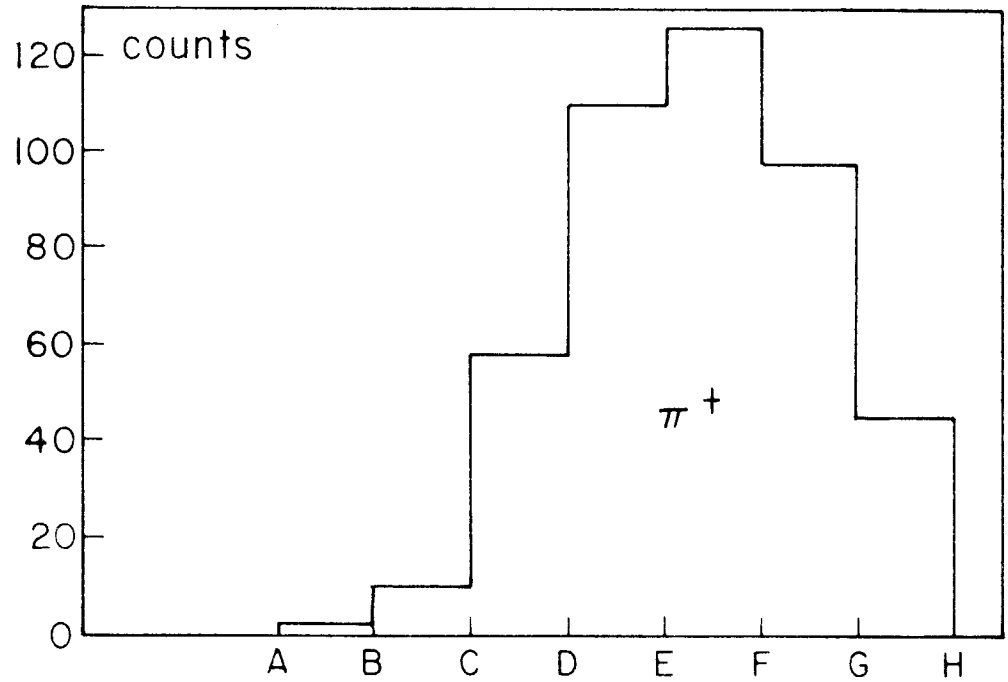

Fulse amplitude (channel width ~ 20v)

b)

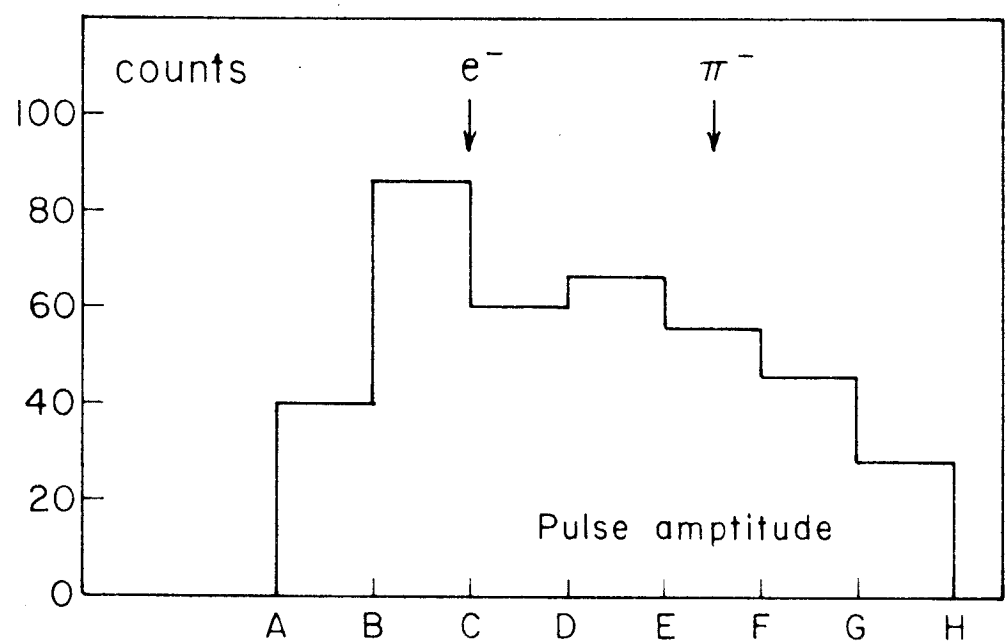

pion is 50 Mev. However, a 100 Mev meson is only 15 °/o above minimum and discrimination becomes very difficult.

In this experiment, discrimination against electrons has been achieved by means of a Čerenkov counter. A particle traveling in a medium of index of refraction n will emit Čerenkov light whenever its velocity exceeds c/n the velocity of light in the medium. The Čerenkov light is emitted at an angle θ from the trajectory of the particle given by $\cos\theta = 1/n\beta$, βc being the velocity of the particle. The intensity of the light is proportional to $\sin^2\theta$. If a rectangular block of lucite ($n = 1.5$), is used as a detector and if the incident particle is normal to one face, then for $\beta > 0.9$ the Čerenkov light is totally reflected on all faces and consequently the light collection efficiency is expected to be good even for a large size counter (there is optical contact between the photomultiplier and the counter and the Čerenkov light can strike the photocathode). On the other hand, if the velocity of the particle is below threshold or only slightly above, its signal will be small for two reasons: first, little light is emitted ($\sin^2\theta$ law) and second the light collection efficiency is poor (no total reflection). Whenever the detection efficiency of a Čerenkov counter is appreciably different for a meson and an electron at a given momentum, separation between pions and electrons can be achieved.

In the range of momenta selected by the spectrometer, the electrons are always ultra-relativistic and the efficiency of the Čerenkov counter for electrons is not expected to vary with electron energy. This efficiency has been measured using the electrons emitted from a lead

target at a laboratory angle of 60°, the spectrometer selecting pions with too small an energy to penetrate the three counters. An efficiency of 70 °/o was found, which was considered suspiciously low since previous tests have indicated nearly 100 °/o efficiency for cosmic-ray mesons. The measurements were repeated after completion of the experiment, this time at an angle of 35° where a practically pure beam of electrons can be achieved from a lead target. The previous result of 70 °/o was confirmed, the discrepancy with the measurements from cosmic rays being due to two main causes:

(1) The gain of the photomultipliers had decreased slightly subsequent to the cosmic-ray test so that some pulses were below the coincidence bias (an efficiency of 83 °/o could be achieved in these runs by lowering the bias).

(2) Some electrons interact in the lead absorbers placed between the scintillation counters (about one radiation length), and miss the Čerenkov counter. By removing the lead absorbers and lowering the anti-coincidence bias, an efficiency of 95 °/o for electrons could be reached, in agreement with the results obtained in the early cosmic-ray test. The residual unaccounted for 5 °/o were probably due to statistical fluctuations in the light collection and scattering of electrons in the scintillation counters. Meson contamination was believed to be less than 2 °/o.

The efficiency of the Čerenkov counter for pions was measured by detecting positive pions from hydrogen. Assuming that the electron

background is negligible will give a first estimate of the Čerenkov efficiency ε_{π}^{o}. The electron background can be measured by changing the polarity of the magnet. Now, the numbers of electrons and negative pions will be of the same order of magnitude and can be calculated from ε_{π}^{o} and the Čerenkov efficiency for electrons. It is then reasonable to assume that the numbers of electrons and positrons are equal and a corrected value of the efficiency for pions can be deduced from the results of the positive pions run. This procedure can be iterated to achieve greater accuracy but in practice, due to the smallness of the positron background it has to be carried out but once. If n_c is the number of quadruple coincidences and n_3 the number of triple coincidences from pion pulses in the scintillation counters for a given run then $\varepsilon_{\pi} = n_c/n_3$. The error in ε_{π} is calculated from a binomial distribution since n_c and n_3 are obtained simultaneously.

The efficiency of the Čerenkov counter for pions is plotted in figure 10a as a function of the pion kinetic energy. There is a 1 % residual efficiency at threshold ($T \sim 55$ Mev) which might come from scintillation of the lucite, electrons from $\pi - \mu - e$ decay chain or other contamination of the pion beam. In order to check that there is no change in efficiency with time, measurements for 125 Mev pions were performed at frequent intervals. Figure 10b shows the result of those measurements. Within statistical errors, no drift of the Čerenkov efficiencies can be detected.

It is interesting to note for future experiments that the Čerenkov efficiency for high-energy pions ($T \sim 150$ Mev) is quite sensitive to the

Figure 10a. Efficiency of the Čerenkov Counter for Pions.

Figure 10b. Efficiency of the Čerenkov Counter for 125 Mev Pions as a Function of Time.

a)

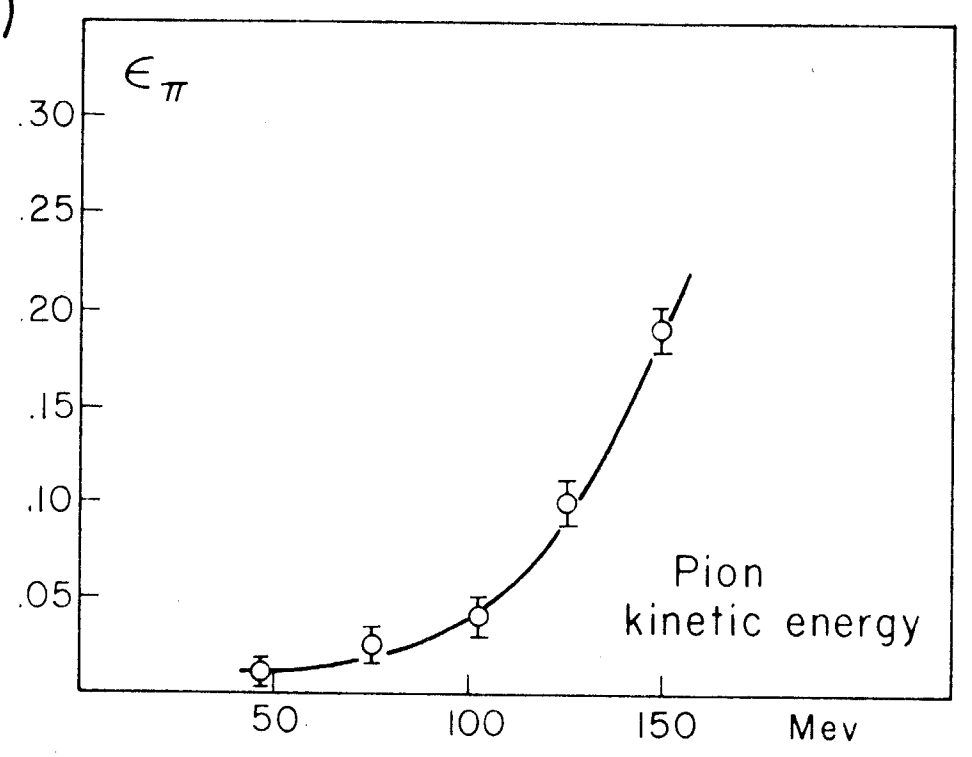
ϵ_π
.30
.25
.20
.15
.10
.05
Pion
kinetic energy
50
100
150
Mev

b)

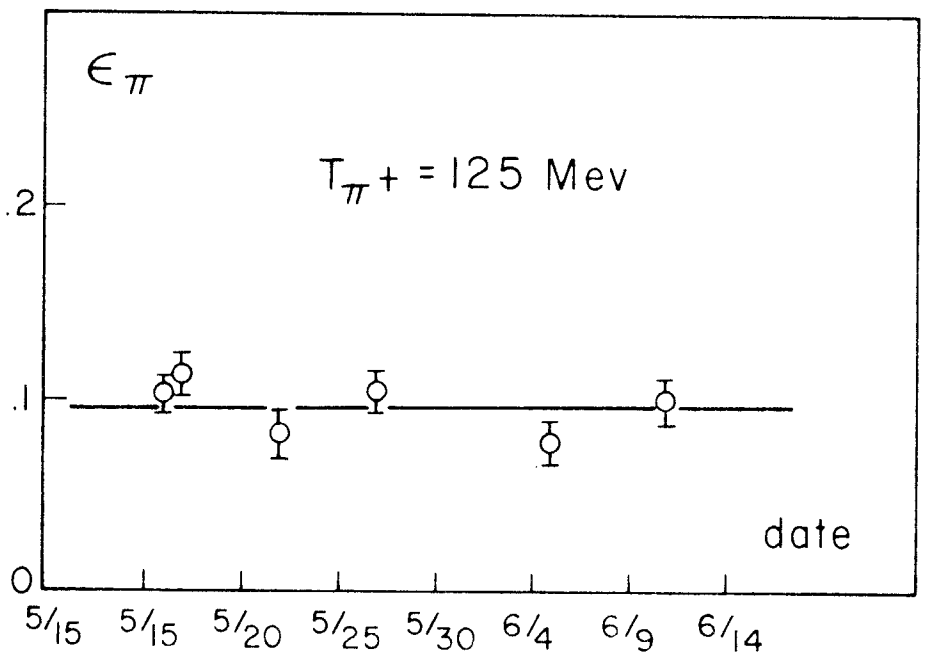
ϵ_π
T_{π^+} = 125 Mev
.2
.1
0
date
5/15
5/15
5/20
5/25
5/30
6/4
6/9
6/14

gain of the photomultipliers in the Čerenkov counter. Decreasing this gain would in general decrease the efficiency for pions to a greater extent than the efficiency for electrons. An optimum gain can be worked out which would depend on the relative proportion of pions and electrons to be separated.

C. Operations

A complete set of data was taken for pions emitted at a laboratory angle of 60^{o} before changing the angular setting to 120^{o}, because the changeover involved moving a considerable amount of lead shielding and equipment.

The maximum photon energy in the bremsstrahlung was obtained from a measurement of the magnetic field in the synchrotron at the time the electrons strike the internal radiator. This photon energy was measured several times daily when runs were in progress, along with the barometric pressure and ionization chamber temperature. When running with hydrogen in the target, measurements of the density were performed at frequent intervals.

Runs with hydrogen in the target and background runs were taken as close in time as possible. Background runs were obtained by leaving in the target only one atmosphere of hydrogen at room temperature. The density is then about 400 times less than in a typical hydrogen run. The counting rate on the background runs was fairly small, in most cases less than 10 $^{o}/o$ of the corresponding rate on hydrogen runs.

The increase in the number of mesons when hydrogen is added to the target may not be due only to pions produced in the hydrogen. The

hydrogen itself may also change the counting rate due to negative pions produced elsewhere. For example, a negative pion can be produced from a neutron in the steel end of the target and then be scattered by the hydrogen into the spectrometer, or a photon from the decay of a neutral pion produced in the hydrogen can create a negative pion in the shielding material or the walls of the target. Estimates of such effects show that they are vanishingly small, (less than 0.1 $^{o}/o$ of the negative pion counting rate), because they involve the product of two small cross-sections (one production and one scattering for instance). These sources of background have been neglected in the reduction of the data. An experimental check on that assumption comes from the fact that negative pion photoproduction goes to zero within the statistical errors for pion energies greater than the maximum energy allowable from kinematics.

A correction must be made for negative pions produced in the impurities of the hydrogen gas. An analysis of the hydrogen indicated 0.1 mole per cent of oxygen and nitrogen (see preceeding section). Littauer and Walker (20) had shown that the ratio of the yield of 65 Mev negative pions in oxygen to the yield of 65 Mev positive pions in hydrogen is about 4. A similar result is expected in nitrogen and an appropriate correction can then be made for the contribution of impurities in hydrogen if it is assumed that the result above is independent of the energy of the pion in the range 50-150 Mev. The correction depends on the angle and energy of the detected pions and is about 3 $^{o}/o$ of the negative pion yield from multiple production at a

bremsstrahlung cut-off energy of 1080 Mev.

The axis of the telescope is horizontal. Due to the large size of the counters, the cosmic-ray counting rate, although small, is not entirely negligible. The total gate-on time of each run was obtained from the "time" counter (Part II. Section F) and the rate of cosmic ray counts was obtained by long runs made when the synchrotron was not operating.

The "singles" counting rate of each counter was low enough so that the accidental coincidences (i.e. a coincidence which is not caused by one particle) represented only a small correction in most cases. A modification of the coincidence circuit made it possible to count coincidences of the pulses from counter 3 with coincidences from counters 1 and 2 after a delay of 2.5 μsec. The indications of this monitor do not give the actual number of the chance coincidences since an accidental coincidence of a pulse from counter 1 with a (2.3) coincidence, for instance, does not trigger the monitor. The correction factor for such effects (the ratio of the actual number of accidentals to the monitor indication) depends on the details of the distribution in time of the beam intensity and not only on its average intensity. It is shown in Appendix I that this correction factor is close to 2 in practice, and since the correction due to accidentals is only a few per cent, a uniform value of 2 for the correction factor was used in the reduction of all the data.

IV. ANALYSIS OF THE DATA

A. Introduction

At the end of a given run the following data have been collected: (1) Information pertaining to the x-ray beam; number of "bips" which is proportional to the total energy flux in the beam; maximum photon energy; barometric pressure and temperature of the ionization chamber. (The ratio of the energy in a "bip" under ordinary laboratory temperature and barometric pressure to the energy in a "bip" under STP conditions turns out to be 1.13 within 0.5 $^{o}/o$. Some early runs were taken without T and P measurements and the factor 1.13 was used in the reduction of the corresponding data.)

(2) Information pertaining to the target: pressure and temperature of the hydrogen gas. From these, one can obtain the density of hydrogen which is proportional to the number of interacting protons.

(3) Information pertaining to the reaction under study: number of triple coincidences with or without a corresponding coincidence from the Čerenkov counter; duration of the run; number of accidental coincidences and pulse height analysis of the pulses from one of the scintillation counter.

In section B it will be shown how these raw data were used to obtain the number of negative pions from hydrogen computed for convenience per "bip" and for a hydrogen density of 0.030.

From the pion counting rate at a given pion energy and bremsstrahlung cut-off energy, the integral of the corresponding cross-section over photon energy can be calculated. This is done in section C.

The results are normalized to an energy flux in the beam equal to the maximum photon energy and sometimes are referred to in the literature as "cross-sections per equivalent quantum". However this name is somewhat misleading, the name "yields per equivalent quantum" will be used here and denoted by σ^*.

In section D the cross-section will be obtained from the yields by a subtraction method.

Finally in section E an analysis of the results obtained from positive pions will be made. Detection of positive pions was performed to check the counting equipment and especially the Čerenkov counter. In addition a run was made at 500 Mev to relate the negative pion yields to single production cross-sections. No cross-section for positive pions multiple production can be obtained accurately because of the large contribution, in the yields, from single production. However some information on multiple production can be deduced from an increase of the yields with increasing bremsstrahlung cut-off energy.

B. Pion Counting Rate

Let n_3 be the number of (123) coincidences during a run, n_c and n_a the number of (1234) and (123-4) coincidences respectively where 1, 2, 3 refer to the three scintillation counters, 4 to the Čerenkov counter. Also call ε_e and ε_π the efficiencies of the Čerenkov counter for the electrons and pions which trigger the three scintillation counters. If n_e and n_π are the numbers of electrons and pions counted during this run, the following relations are obtained:

$$n_3 = n_e + n_\pi$$

$$n_3 = n_c + n_a$$

$$n_c = \varepsilon_e n_e + \varepsilon_\pi n_\pi$$

It is convenient to express n_π and n_e as functions of n_c and n_a since the latter quantities are statistically independent. From the relations above:

$$n_\pi = \frac{\varepsilon_e}{\varepsilon_e - \varepsilon_\pi}\left[n_a - \frac{1 - \varepsilon_e}{\varepsilon_e} n_c\right] \tag{1}$$

$$n_e = \frac{\varepsilon_\pi}{\varepsilon_\pi - \varepsilon_e}\left[n_a - \frac{1 - \varepsilon_\pi}{\varepsilon_\pi} n_c\right] \tag{2}$$

Define $\alpha = \frac{\varepsilon_e}{\varepsilon_e - \varepsilon_\pi}$, $\beta = \frac{\varepsilon_e - 1}{\varepsilon_e - \varepsilon_\pi}$, then

$$n_\pi = \alpha n_a + \beta n_c \tag{1'}$$

The statistical error on n_π, Δn_π, can be found from the relation:

$$\left(\Delta n_\pi\right)^2 = \left(\frac{\partial n_\pi}{\partial n_a} \Delta n_a\right)^2 + \left(\frac{\partial n_\pi}{\partial n_c} \Delta n_c\right)^2 + \left(\frac{\partial n_\pi}{\partial \varepsilon_\pi} \Delta \varepsilon_\pi\right)^2 + \left(\frac{\partial n_\pi}{\partial \varepsilon_e} \Delta \varepsilon_e\right)^2$$

or

$$\left(\Delta n_\pi\right)^2 = \alpha^2\left(\Delta n_a\right)^2 + \beta^2\left(\Delta n_c\right)^2 + \frac{1}{\left(\varepsilon_e - \varepsilon_\pi\right)^2}\left[n_\pi^2\left(\Delta\varepsilon_\pi\right)^2 + n_e^2\left(\Delta\varepsilon_e\right)^2\right] \tag{3}$$

where Δn_a, Δn_c are obtained from the counting statistics on n_a and n_c; $\Delta\varepsilon_\pi$ and $\Delta\varepsilon_e$ are obtained from the experimental errors in the determination of ε_π and ε_e. Table I shows the values of ε_π, ε_e, α, β, $\Delta\varepsilon_\pi$, $\Delta\varepsilon_e$ for the different pion energies studied in this experiment. The pion energies quoted in Table I are the energies inside the target. Energy losses, in the steel walls of the target, of 1.5 Mev for the 50 Mev pions and about 1 Mev for the 100 and 150 Mev pions were taken into account.

The pion energies were reproducible to better than 1 °/o during the different runs for a particular experimental point, but hydrogen densities and maximum bremsstrahlung energies could vary. In order to obtain the quantities n_a and n_c per "bip" at a particular bremsstrahlung cut-off energy, the total numbers of (123-4) and (1234) coincidences for all the runs taken at approximately the same maximum photon energy were first corrected for accidental and cosmic-ray coincidences and then divided by the total number of "bips". A mean density $\langle\rho\rangle$ and mean bremsstrahlung cut-off energy, $\langle k_{max}\rangle$ were obtained by a weighted average, the weighing factor being the number of "bips" for each run. In most cases the variation in photon

TABLE I.

Efficiencies of the Čerenkov Counter

T_π	ε_e	$\Delta\varepsilon_e$	ε_π	$\Delta\varepsilon_\pi$	α	$-\beta$
50	0.70	0.02	0.01	0.01	1.015	0.435
77*	0.68	0.02	0.01	0.01	1.015	0.475
103	0.70	0.02	0.04	0.01	1.06	0.455
124*	0.68	0.02	0.04	0.01	1.06	0.500
147	0.70	0.02	0.19	0.01	1.37	0.590

* Runs at these energies were made about a month after the rest of the data were taken. The gains of the photomultipliers have decreased slightly.

energy was less than 5 Mev. Background runs were treated similarly.

Tables II and III show the raw data for hydrogen and background runs taken at laboratory angles of 60^{o} and 120^{o} respectively. The results are expressed "per bip" along with the corresponding mean values for the density and maximum photon energy. Although the mean value of the bremsstrahlung energy for background runs sometimes differs slightly from the corresponding value for hydrogen runs, it is not indicated in the tables because the background results are small and vary little with photon energy. Background results are then simply subtracted from hydrogen runs results and the number of pions are obtained from equation 1'. The last column in the tables II and III shows the number of negative pions "per bip" normalized to a hydrogen density of 0.030. It must be noted that the "bip" used here is obtained directly from the current integrator. Its value in terms of beam energy flux will depend on the maximum bremsstrahlung cut-off energy (see Part II section E). Also, for convenience, the value of the bip is chosen to be 1.13 times its value under STP conditions. The errors quoted in the number of pions include counting statistics and errors due to uncertainties in Čerenkov efficiencies.

C. Negative Pion Yields

Let $\sigma_{T,\theta}(k)$ be the differential cross-section for production in hydrogen, by a photon of energy k, of a negative pion emitted with a kinetic energy T at a laboratory angle θ. The relation between the counting rate of pions, C_{-}, obtained in the previous section, and the

TABLE II.

Counting Rates per "bip" at $\theta = 60^{\circ}$

$\langle k_{max} \rangle$	T_π Mev	$n_a(H_2)$	$n_c(H_2)$	$n_a(BG)$	$n_c(BG)$	$\langle \rho \rangle$	n_π
1080	50	2.17 ± 0.05	0.82 ± 0.03	0.12 ± 0.035	0.15 ± 0.03	0.0313	1.73 ± 0.075
1080	103	3.40 ± 0.075	0.76 ± 0.035	0.14 ± 0.035	0.05 ± 0.03	0.0312	3.00 ± 0.105
1080	147	2.98 ± 0.075	1.12 ± 0.045	0.10 ± 0.06	0.00 ± 0.05	0.0312	3.16 ± 0.14
920	50	2.18 ± 0.06	0.92 ± 0.045	0.14 ± 0.02	0.16 ± 0.03	0.0306	1.71 ± 0.08
920	103	3.26 ± 0.075	0.82 ± 0.04	0.19 ± 0.06	0.06 ± 0.05	0.0301	2.89 ± 0.115
920	147	2.45 ± 0.075	1.03 ± 0.05	0.11 ± 0.05	0.00 ± 0.05	0.0302	2.58 ± 0.125
720	50	2.06 ± 0.065	0.91 ± 0.045	0.10 ± 0.05	0.19 ± 0.06	0.0300	1.68 ± 0.095
720	103	2.57 ± 0.075	0.65 ± 0.045	0.03 ± 0.05	0.01 ± 0.04	0.0300	2.40 ± 0.105
720	147	1.39 ± 0.055	0.59 ± 0.045	-0.05 ± 0.08	0.00 ± 0.10	0.0300	1.55 ± 0.145
610	50	1.61 ± 0.13	0.87 ± 0.10	Not measured.		0.0298	1.15 ± 0.165
610	103	0.84 ± 0.15	0.52 ± 0.13	720 Mev background was		0.0304	0.62 ± 0.185
610	147	0.34 ± 0.12	0.33 ± 0.13	used		0.0304	0.27 ± 0.21

TABLE III.

Counting Rates per "bip" at $\theta = 120^{\circ}$

$\langle k_{max} \rangle$	T_π Mev	$n_a(H_2)$	$n_c(H_2)$	$n_a(BG)$	$n_c(BG)$	$\langle \rho \rangle$	n_π
1090	50	0.99 ± 0.04	0.25 ± 0.025	0.14 ± 0.03	0.02 ± 0.02	0.0283	0.81 ± 0.06
1080	77	1.32 ± 0.06	0.11 ± 0.025	0.18 ± 0.045	0.05 ± 0.04	0.0288	1.13 ± 0.08
1090	103	0.98 ± 0.045	0.12 ± 0.025	0.18 ± 0.04	0.04 ± 0.025	0.0278	0.87 ± 0.07
1080	124	0.65 ± 0.035	0.08 ± 0.02	0.17 ± 0.045	0.02 ± 0.025	0.0989	0.50 ± 0.06
1090	147	0.32 ± 0.030	0.12 ± 0.02	0.06 ± 0.05	0.03 ± 0.03	0.0290	0.32 ± 0.08
935	50	1.00 ± 0.045	0.23 ± 0.03	0.14 ± 0.03	0.02 ± 0.025	0.0302	0.77 ± 0.06
940	77	1.15 ± 0.07	0.14 ± 0.035	0.14 ± 0.05	-0.01 ± 0.025	0.0296	0.98 ± 0.10
935	103	0.84 ± 0.05	0.11 ± 0.025	0.16 ± 0.045	0.02 ± 0.03	0.0304	0.67 ± 0.07
940	124	0.49 ± 0.035	0.07 ± 0.02	0.07 ± 0.03	0.00 ± 0.025	0.0296	0.43 ± 0.055
935	147	0.19 ± 0.035	0.14 ± 0.03	0.03 ± 0.045	0.08 ± 0.03	0.0305	0.17 ± 0.05
720	50	0.69 ± 0.05	0.16 ± 0.035	0.19 ± 0.06	-0.08 ± 0.06	0.0307	0.43 ± 0.085
720	103	0.35 ± 0.045	0.05 ± 0.095	0.13 ± 0.05	-0.05 ± 0.04	0.0307	0.20 ± 0.075
720	147	0.09 ± 0.08	0.04 ± 0.08	0.13 ± 0.075	0.05 ± 0.007	0.0309	-0.04 ± 0.18

cross-section $\sigma_{T,\theta}(k)$ can be expressed by:

$$C_- = \eta \mathcal{N} \Delta\Omega \, \Delta T \int_0^E N(k) \, \sigma_{T,\theta}(k) \, dk \qquad (4)$$

where:

C = pion counting rate per bip

η = pion counting efficiency

$\mathcal{N}$ = number of protons per $cm.^2$ in the useful volume of the target

$\Delta\Omega$ = laboratory solid angle of acceptance by the spectrometer

ΔT = range of pion energies accepted by the spectrometer

$N(k)dk$ = number of photons of energy k (within dk) per bip

E = bremsstrahlung cut-off energy.

If $B(k)$ is defined as in Part II such that $\int_0^E B(k)\, dk = E$ then

$N(k) = Q\, B(k)/k$ with Q = (energy in a bip)/E (5)

The yield "per equivalent quantum" is by definition:

$$\sigma^*_{T,\theta}(E) = \int_0^E B(k)/k \; dk \; \sigma_{T,\theta}(k) \qquad (6)$$

The relation between counting rate and yield is then:

$$C_- = \eta \mathcal{N} \Delta\Omega \, \Delta T \, Q \, \sigma^* \qquad (7)$$

The experimental parameters η, $\mathcal{N}$, $\Delta\Omega$, ΔT can be calculated for each measurement. However, some of them are difficult to obtain with accuracy. For example, η contains a π - μ decay correction

complicated by the fact that μ mesons cannot be distinguished from pions by the counters. This correction has not yet been calculated very accurately and only estimates can be given for it. For more details on this problem refer to Appendix II. Similarly, other factors such as slit penetration, scattering on the lead bridges, useful volume of the target cannot be calculated with precision.

It is therefore convenient to relate the yields of negative pions to a cross-section which has already been obtained, namely a single photoproduction cross-section of positive pion in hydrogen. By inverting the polarity of the field of the analysing magnet and by operating the synchrotron at 500 Mev, positive pions are detected with a negligible contamination from pair production. For single photoproduction of positive pions, the relation between counting rate and the cross-section is:

$$C_+ = \eta \eta \Delta\Omega \, N(k) \, \Delta k \, \sigma^+_\theta \tag{8}$$

where σ^+_θ is the differential cross-section at a laboratory angle of θ. $N(k)\Delta k$ is the number of interacting photons and is related to the pion energy acceptance of the spectrometer by the relation: $\Delta k = \Delta T \frac{dk}{dT}$ where dk/dT is given by the kinematics of the reaction. Using equation 4:

$$C_+ = (\eta \eta \Delta\Omega \Delta T Q) \quad \frac{B(k)}{k} \quad \frac{dk}{dT} \quad \sigma^+_\theta \tag{8'}$$

Since a given angle and energy of the positive pion determine the energy of the interacting photon, the factor $\frac{B(k)}{k} \, dk/dT$ can be calculated.

The value of σ^{+}_{θ} can be obtained by interpolation from the results of the Caltech group (21).

Call $$K = \eta \mathcal{N} \Delta\Omega \Delta T Q \tag{9}$$

or since $$\Delta T = p\beta \frac{\Delta p}{p}, \quad K = \eta Q p \beta \left(\mathcal{N} \Delta\Omega \frac{\Delta p}{p}\right) \tag{9'}$$

where p = pion momentum and βc = pion velocity. The quantities between parenthesis depend only on the target and the spectrometer parameters. On the other hand the remaining quantities depend on the maximum photon energy and the energy of the analysed pion. The pion energy dependence of η is due mostly to pion decay correction and can be calculated approximately (see Appendix II). The π-μ decay correction depends on the shape of the pion energy spectrum which is different for π^{+} and π^{-}. Fortunately the spectra are close enough that the effect on the correction is less than 1 $^{o}/o$. The dependence of Q on bremsstrahlung cut-off energy is obtained by beam calibration (see Part II Section E). The positive pion run was performed at a laboratory angle of 60^{o}, the machine energy E_{+} being 493 Mev. The pion kinetic energy chosen (T_{+} = 125 Mev) corresponds to the resonance in the photoproduction of single pions at that particular angle. From equation 8' the quantity $K(T_{+}, E_{+})$ can be determined using the experimental counting rate C_{+} and the value of the cross-section $\sigma^{+}_{\theta} = 2.13 \times 10^{-29}$ cm^{2}/ster from Caltech results (21). The quantity K(T, E) can then be obtained from equation 9' by the relation:

$$K(T, E) = K(T_+, E_+) \frac{(\eta Qp\beta)_{T,E}}{(\eta Qp\beta)_{T_+, E_+}} \tag{10}$$

since the dependence of $(\eta Qp\beta)$ on T and E can be estimated from equation 5 and the results of $\pi^- \mu$ decay correction. Table IV gives K(T, E) for the different values of T and E considered in this experiment.

Equation 7 can then be written:

$$\sigma^*_{T,\theta}(E) = \frac{C_-(\theta, T, E)}{K(\theta, T, E)} \tag{7'}$$

The values of the yields per equivalent quantum for negative pions emitted at a laboratory angle of 60^o are tabulated in Table V, the yields for negative pions emitted at 120^o are tabulated in Table VI. In obtaining the yields from equation 7', the negative pions produced in the small amount of impurities in the hydrogen have been subtracted from the pion counting rate listed in Tables II and III. The ratio of the negative pion counting rate from impurities to the positive pion counting rate from hydrogen is approximately 4×10^{-3} and the positive pion counting rate was estimated from the results listed in reference 21.

The errors quoted in Tables V and VI include counting statistics and errors in the determination of the Čerenkov efficiencies. In addition, since the negative pion yields are obtained relative to a single pion photoproduction cross-section, any error on the determination of that cross-section will reflect directly on the magnitude of the yields.

TABLE IV.

E	T_π	$\frac{\eta}{\eta_+}$	$\frac{Q}{Q_+}$	$\frac{p\beta}{p_+\beta_+}$	$\frac{K(T,E)}{K(T_+E_+)}$	K(T,E)
1080	50	0.89	0.518	0.445	0.205	0.80
1080	77	0.945	0.518	0.658	0.323	1.26
1080	103	0.98	0.518	0.840	0.427	1.66
1080	124	1.00	0.518	0.990	0.518	2.00
1080	147	1.02	0.518	1.138	0.600	2.34
920	50	0.89	0.604	0.445	0.239	0.935
935	50	0.89	0.594	0.445	0.236	0.92
935	77	0.945	0.594	0.658	0.370	1.44
920	103	0.98	0.604	0.840	0.495	1.935
935	103	0.98	0.594	0.840	0.489	1.90
935	124	1.00	0.594	0.990	0.594	2.30
920	147	1.02	0.604	1.138	0.700	2.73
935	147	1.02	0.594	1.138	0.690	2.68
720	50	0.89	0.741	0.445	0.294	1.145
720	103	0.98	0.791	0.84	0.609	2.38
720	147	1.02	0.741	1.138	0.861	3.35
610	50	0.89	0.849	0.445	0.337	1.31
610	103	0.98	0.849	0.840	0.699	2.27
610	147	1.02	0.849	1.138	0.985	3.83

TABLE V.

Yields per Equivalent Quantum at 60^{o}
(in units of $10^{-32} cm^{2}$/ster-Mev)

E(Mev)	T(Mev)	$\sigma^{*}_{T,\theta}$
1080	50	2.14 ± 0.005
1080	103	1.77 ± 0.065
1080	147	1.32 ± 0.06
920	50	1.81 ± 0.085
920	103	1.46 ± 0.06
920	147	0.92 ± 0.045
720	50	1.45 ± 0.085
720	103	0.97 ± 0.045
720	147	0.43 ± 0.045
610	50	0.86 ± 0.125
610	103	0.20 ± 0.07
610	143	0.04 ± 0.05

TABLE VI.

Yields per Equivalent Quantum at 120^{o}
(in units of $10^{-32} cm^{2}$/ster-Mev)

E(Mev)	T(Mev)	$\sigma^{*}_{T,\theta}$
1090	50	0.98 ± 0.075
1080	77	0.76 ± 0.055
1090	103	0.50 ± 0.04
1080	124	0.25 ± 0.03
1090	147	0.13 ± 0.035
935	50	0.81 ± 0.065
940	77	0.63 ± 0.07
935	103	0.33 ± 0.035
940	124	0.18 ± 0.025
935	147	0.06 ± 0.02
720	50	0.34 ± 0.075
720	103	0.06 ± 0.03
720	147	-0.01 ± 0.035

The statistical error on the positive pion counting rate is about 3 °/o and the uncertainty on σ_θ^+ is quoted to be about 8 °/o.

Additional errors come from hydrogen density measurement uncertainties (3 °/o) and calibration of the ionization chamber (1 °/o). Other corrections which would enter directly in an absolute determination of the yields are greatly reduced by making a relative measurement. They are slit penetration, scattering on the lead bridges, absorption in the counters and lead absorbers and $\pi - \mu$ decay corrections. The residual errors due to these causes which occur because the negative pion energy and energy spectrum may differ from the energy and energy spectrum of the positive pion, can be estimated to be less than 3 °/o.

The experimental parameters were nearly the same for the data taken at 60° and 120° because the two experimental lay-outs were carefully made symmetric with respect to a plane perpendicular to the beam direction and passing through the center of the target. The correction to the negative pion yields at 120° which arises from possible variations of the experimental parameters (slit width, distance magnet to target etc.) is less than 2 °/o.

As a consistency check, a direct calculation of the positive pion cross-section was performed by using the known values of the experimental parameters together with estimates of the $\pi - \mu$ decay correction, slit penetration and absorption corrections. The result of this calculation is $\sigma_\theta^+ = (2.20 \pm 0.26) \times 10^{-29} \text{cm}^2/\text{ster}$. where the quoted error comes mostly from difficulties in estimating absolute counting corrections. This result is in agreement, within statistical errors, with the

value of the cross-section obtained in a earlier experiment (21)

$\sigma_\theta^+ = (2.13 \pm 0.17) \times 10^{-29}$ cm^2/ster.

D. Determination of the Cross-Sections

Consider the yields per effective quantum obtained at two different bremsstrahlung cut-off energies E_1 and E_2 where $E_2 > E_1$. Using equation 6 from the preceding section:

$$\sigma^*(T, E_2) - \sigma^*(T, E_1) = \int_0^{E_2} B(E_2, k)\, \sigma_{T,\theta}(k)dk/k - \int_0^{E_1} B(E_1, k)\sigma_{T,\theta}(k)dk/k$$

or

$$\sigma^*(T, E_2) - \sigma^*(T, E_1) = \int_0^{E_2} R(k)\, \sigma_{T,\theta}(k)dk/k \qquad (11)$$

where a photon energy resolution R(k) is defined by:

$$R(k) = B(E_2, k) - B(E_1, k) \qquad (12)$$

and $\sigma_{T,\theta}(k)$ is the differential cross-section defined in the preceding section. In figure 11a the functions B(E, k) are plotted for E = 610, 720, 920 and 1080 Mev and in figure 11b the resolution function R(k) is plotted for E_1 = 920 Mev and E_2 = 1080 Mev.

The photon energy threshold for pion multiple photoproduction is about 400 Mev and the cross-sections $\sigma_{T,\theta}(k)$ are very small below a photon energy of 600 Mev. It can be seen from figure 11b, that the increase in yield when the machine energy is raised from E_1 to E_2 comes nearly exclusively from photons in the range of energies

Figure 11a. Bremsstrahlung Spectra Normalized "Per Equivalent Quantum" for the Different Values of E_o used in this Experiment.

Figure 11b. Photon Energy Resolution for E_1 = 920 Mev and E_2 = 1080 Mev.

a)

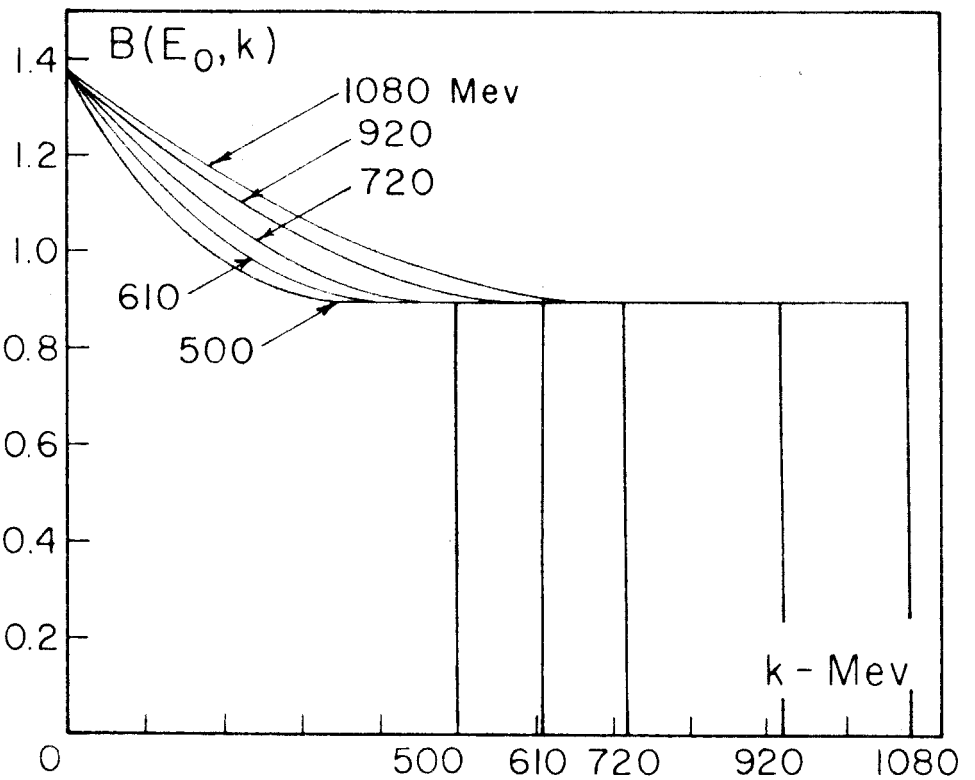
B(E0, k)
1080 Mev
920
720
610
500
1.4
1.2
1.0
0.8
0.6
0.4
0.2
0
k - Mev
500
610
720
920
1080

b)

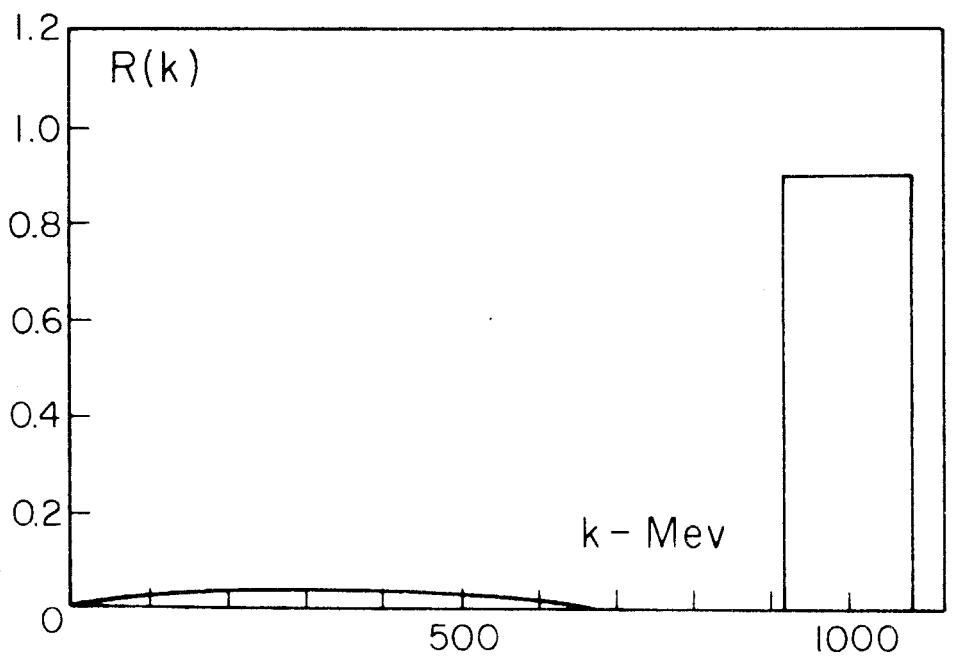
R(k)
1.2
1.0
0.8
0.6
0.4
0.2
0
k - Mev
500
1000

between E_1 and E_2. The contribution of the photons of energies below 600 Mev can be estimated to be negligible.

Equation 11 can then be written:

$$\sigma^*(T, E_2) - \sigma^*(T, E_1) \sim \int_{E_1}^{E_2} R(k)\, \sigma_{T,\theta}(k)\, dk/k$$

and if it is assumed that $\sigma_{T,\theta}(k)$ is a slowly varying function of k

$$\sigma^*(T, E_2) - \sigma^*(T, E_1) \sim \frac{R(\bar{k})}{\bar{k}}\, \sigma_{T,\theta}(\bar{k})\, \Delta k \qquad (13)$$

where: $R(\bar{k}) = 0.9$ in this experiment

$$\bar{k} = 1/2(E_1 + E_2)$$

$$\Delta k = E_2 - E_1$$

The cross-sections for photoproduction of negative pions from hydrogen can then be obtained by the relation:

$$\sigma_{T,\theta}(k) = \frac{\bar{k}}{0.9\, \Delta k} \left[\sigma^*(T, E_2) - \sigma^*(T, E_1) \right] \qquad (13')$$

In order to interpret the results of the experiment and in particular to obtain information on the angular distribution, it is convenient to express the cross-sections in the center of momentum system. The energy of the photon, $\bar{k}$, being known, the velocity of the C.M. system is simply $\beta_o = \bar{k}/(\bar{k} + M)$ where M is the rest mass of the proton.

From the Lorentz transformations it can be shown that:

$$\sigma_{T',\theta'}(CM) = \sigma_{T,\theta}(lab)\,\frac{d\Omega}{d\Omega'}\,\frac{dT}{dT'} = \sigma_{T,\theta}\,\frac{p'}{p} \qquad (14)$$

where the primed quantities are expressed in the C.M. system, p and T being the momentum and kinetic energy of the pion, $d\Omega$ the solid angle of emission of the pion.

The values of the cross-sections expressed both in the laboratory system and the C.M. system are listed in Tables VII and VIII. The pion energy and angle of emission for both systems are also indicated in the tables. The errors quoted include counting statistics and errors due to Čerenkov efficiency uncertainties. It must be pointed out that those errors are <u>not</u> obtained from the errors on the yields listed in Tables V and VI, but are computed directly from the counting rates listed in Tables II and III. From equation 3 it can be seen that the errors due to Čerenkov efficiency uncertainties are much smaller relative to counting statistics in the cross-sections calculation than they are in the case of the yields calculation.

The error in the determination of the hydrogen density from run to run is about 1 °/o. As pointed out in Part II, if the difference between two given yields is small compared to the yields themselves, then the error in the corresponding cross-section due to the uncertainty in the density measurement may become large (it is 10 °/o if the difference is only 10 °/o of the yields). However, the error from counting statistics becomes large under the same conditions and represents

TABLE VII.

Cross-Sections for Negative Pion Photoproduction at $\theta_{lab} = 60^{o}$ (in units of 10^{-32} cm^2/ster-Mev)

$\bar{k}$(Mev)	T(Mev)	$\sigma_{T,\theta}$(lab)	θ'	T'(Mev)	p'/p	$\sigma_{T',\theta'}$(CM)
1000	50	2.30 ± 0.76	110^{o}	42	0.92	2.12 ± 0.70
1000	103	2.10 ± 0.51	100^{o}	83	0.88	1.85 ± 0.45
1000	197	2.78 ± 0.48	97^{o}	119	0.87	2.42 ± 0.42
820	50	1.84 ± 0.51	104^{o}	40	0.89	1.64 ± 0.46
820	103	2.27 ± 0.29	95^{o}	81	0.87	1.97 ± 0.25
820	147	2.20 ± 0.27	92^{o}	118	0.865	1.90 ± 0.23
665	50	3.78 ± 0.91	98^{o}	38	0.87	3.26 ± 0.79
665	103	5.25 ± 0.51	90^{o}	80	0.865	4.55 ± 0.44
665	147	2.62 ± 0.46	88^{o}	118	0.865	2.27 ± 0.40

TABLE VIII

Cross-Sections for Negative Pion Photoproduction at $\theta_{lab} = 120^{o}$ (in units of 10^{-32} cm^2/ster-Mev)

$\bar{k}$ (Mev)	T(Mev)	$\sigma_{T,\theta}$(lab)	θ'	T'(Mev)	p'/p	$\sigma_{T',\theta'}$(CM)
1010	50	1.26 ± 0.57	150^{o}	122	1.71	2.16 ± 0.98
1010	77	1.43 ± 0.60	148^{o}	166	1.63	2.35 ± 0.98
1010	103	1.26 ± 0.36	147^{o}	204	1.58	1.99 ± 0.57
1010	124	0.53 ± 0.29	146^{o}	236	1.55	0.82 ± 0.45
1010	147	0.52 ± 0.24	146^{o}	274	1.54	0.80 ± 0.37
828	50	2.04 ± 0.47	147^{o}	110	1.61	3.28 ± 0.76
828	103	1.11 ± 0.20	144^{o}	187	1.49	1.65 ± 0.39
828	147	0.28 ± 0.26	143^{o}	253	1.45	0.41 ± 0.38
660*	50	2.60 ± 0.70	145^{o}	99	1.50	3.90 ± 1.05
660*	103	0.52 ± 0.26	142^{o}	171	1.40	0.73 ± 0.37

* The cross-sections at this photon energy were obtained by assuming the yields at E_o = 600 Mev to be zero.

in all cases the main uncertainty in the determination of the cross-sections. Because a cross-section is obtained from a difference between two "yields per effective quantum" of pions at the same energy and with nearly the same energy spectrum, the errors due to slit penetration, scattering on lead bridges, $\pi - \mu$ decay correction are negligible compared to the error from counting statistics. It must be also remembered that, like the yields, the cross-sections are expressed relative to a single pion photoproduction cross-section. The absolute magnitude of the negative pion cross-sections is only determined within the accuracy of the single pion photoproduction cross-section used as a reference.

E. Results from Positive Pion Runs

The data obtained when positive pions were detected can be analysed as in the preceding sections. Most of the counting rate however comes from single photoproduction. For a given energy and angle of emission of a positive pion originating from a single photoproduction, the energy of the incident photon can be calculated.

The increase in positive pion yields "per equivalent quantum" when the maximum bremsstrahlung energy is raised from E_1 to E_2 comes from pions produced by photons in the energy range (E_1, E_2) as before, but in addition there is a contribution from pions produced singly if the number of photons at the corresponding "single production" energy varies with the bremsstrahlung cut-off energy. It turns out that this is indeed the case. For example, at 60^o and for pion energy of

125 Mev the incident photon energy is 308 Mev. It can be seen from figure 11b that photons of that energy do contribute to the difference in yields between 1080 and 920 Mev. Fortunately, the cross-sections for single photoproduction are known from previous measurements made in this laboratory (21) and one can calculate the contribution of single photoproduction to the increase in the positive pion yields with increasing bremsstrahlung cut-off energy.

The positive pion yields are listed in Table IX along with the corresponding counting rates per bip normalized to a hydrogen density of 0.030. Since the number of positrons is only about 5 $^{o}/_{o}$ of the number of positive pions, the Čerenkov counter indications were not used to obtain the positive pion counting rates. It was, rather, assumed that the number of positrons was equal to the number of electrons obtained in connection with the negative pion runs. The electron counting rate was simply subtracted from the total triple coincidences counting rate obtained with the scintillation counters alone. The background counting rates were also assumed to be the same for positive and negative particles (they are only about 1 $^{o}/_{o}$ of the positive pion counting rates). The errors listed in Table IX come from counting statistics and are the most important one. The other types of errors indicated in the previous sections are also present here.

In Table X the cross-sections for the positive pions from multiple photoproduction are summarized. Corrections for the positive pions produced in a single photoproduction reaction have been performed. The utility of these data is seriously limited by the rather large statistical errors.

TABLE IX.

Yields per Equivalent Quantum for Positive Pions
(in units of 10^{-32} cm^2/ster-Mev)

k_{max}	θ	T(Mev)	C_+(per bip)	σ_+^*
1080	60°	50	7.95 ± 0.35	9.9 ± 0.45
925	60°	50	9.60 ± 0.35	10.3 ± 0.40
720	60°	50	9.80 ± 0.50	8.6 ± 0.45
1090	60°	125	28.8 ± 0.50	14.3 ± 0.25
920	60°	125	31.4 ± 0.60	13.4 ± 0.26
720	60°	125	32.0 ± 0.75	11.1 ± 0.26
500	60°	125	33.4 ± 1.30	8.7 ± 0.35
1080	120°	50	7.45 ± 0.30	9.3 ± 0.38
935	120°	50	8.25 ± 0.50	9.0 ± 0.55
720	120°	50	8.80 ± 0.60	7.7 ± 0.53
1080	120°	147	3.0 ± 0.90	1.28 ± 0.085
935	120°	147	2.70 ± 0.15	1.01 ± 0.055
790	120°	147	3.35 ± 0.35	1.00 ± 0.105

TABLE X.

Cross-Sections for Multiple Photoproduction of Positive Pions
(in units of 10^{-32} cm^2/ster-Mev)

$\bar{k}$(Mev)	θ	T(Mev)	σ_+ (lab)
1000	60^o	50	-4.2 ± 4.2
1000	60^o	125	3.2 ± 2.5
820	60^o	50	6.1 ± 2.7
820	60^o	125	7.7 ± 1.7
610	60^o	125	5.8 ± 1.3
1010	120^o	50	0.79 ± 4.8
1010	120^o	147	1.7 ± 0.8
830	120^o	50	3.9 ± 3.1
830	120^o	147	-0.04 ± 0.5

V. DISCUSSION OF THE RESULTS

A. Comparison with Previous Experiments

The yields of negative pions obtained at a laboratory angle of 60° are plotted as a function of bremsstrahlung cut-off energy in figure 12a. The yields $\sigma^{*}_{T,\theta}$ are expressed as yields per proton per equivalent quantum and per unit energy and solid angle of the emitted pion. The yields obtained at a laboratory angle of 120° are given in figure 12b.

The results obtained at Stanford and Cornell Universities (6, 8) are also expressed as yields per equivalent quantum and are plotted in figure 13 along with the results of this experiment.

The data from Stanford University were taken at a laboratory angle of 60° and are in agreement with the corresponding data from this experiment. The data from Cornell University were taken at a different angle of emission of the negative pion and cannot be compared directly with our results. It can be seen however, that the qualitative features of both set of results are not in disagreement.

The yields "per equivalent quantum" of positive pions are plotted in figure 14. From equations 7 and 8' of Part IV, the relation between the yields "per equivalent quantum" due to single photoproduction and the corresponding cross-sections is:

$$\sigma^{*}_{+} = \frac{B(E_{o}, k)}{k} \frac{dk}{dT} \sigma_{\theta}{}^{+}$$

where k is the energy of the photon responsible for single production of

Figure 12a. Yields of Negative Pions Obtained at a Laboratory Angle of 60^{o}.

Figure 12b. Yields of Negative Pions Obtained at a Laboratory Angle of 120^{o}.

In both figures the black dots on the bremsstrahlung cut-off energy axis represent the photon energy thresholds for the production of pion pairs with one pion at the required angle and energy.

a)

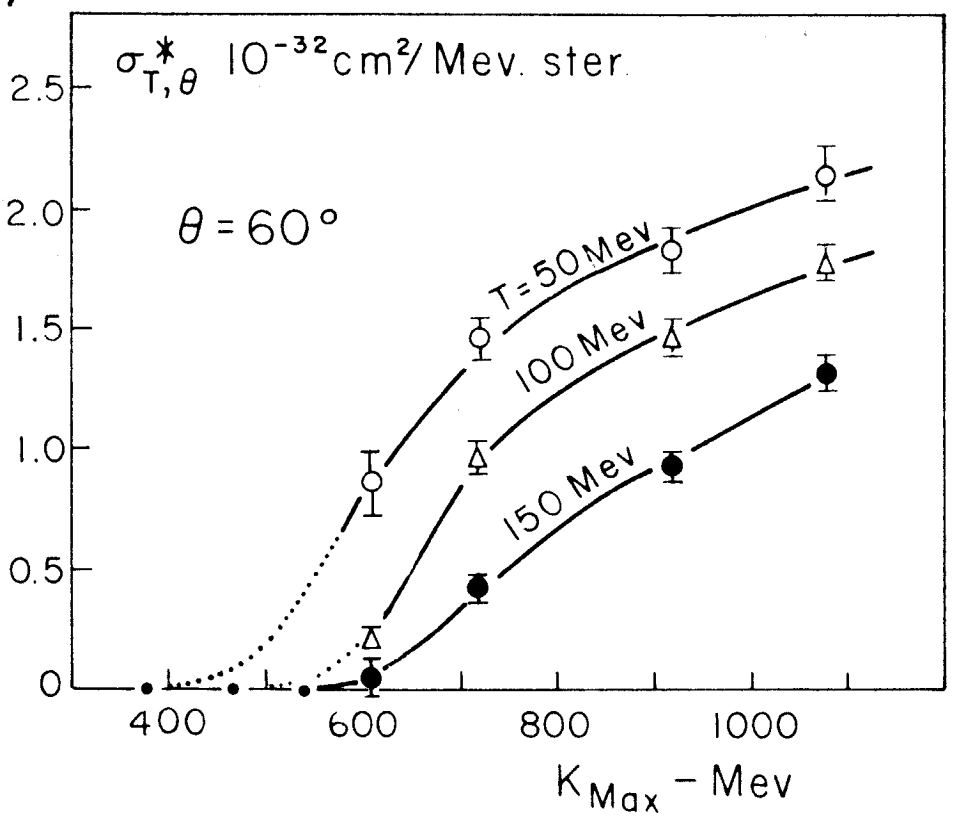
$\sigma^*_{T,\theta}$ 10^{-32}cm²/Mev. ster.
θ = 60°
T=50 Mev
100 Mev
150 Mev
2.5
2.0
1.5
1.0
0.5
0
400
600
800
1000
K_{Max} – Mev

b)

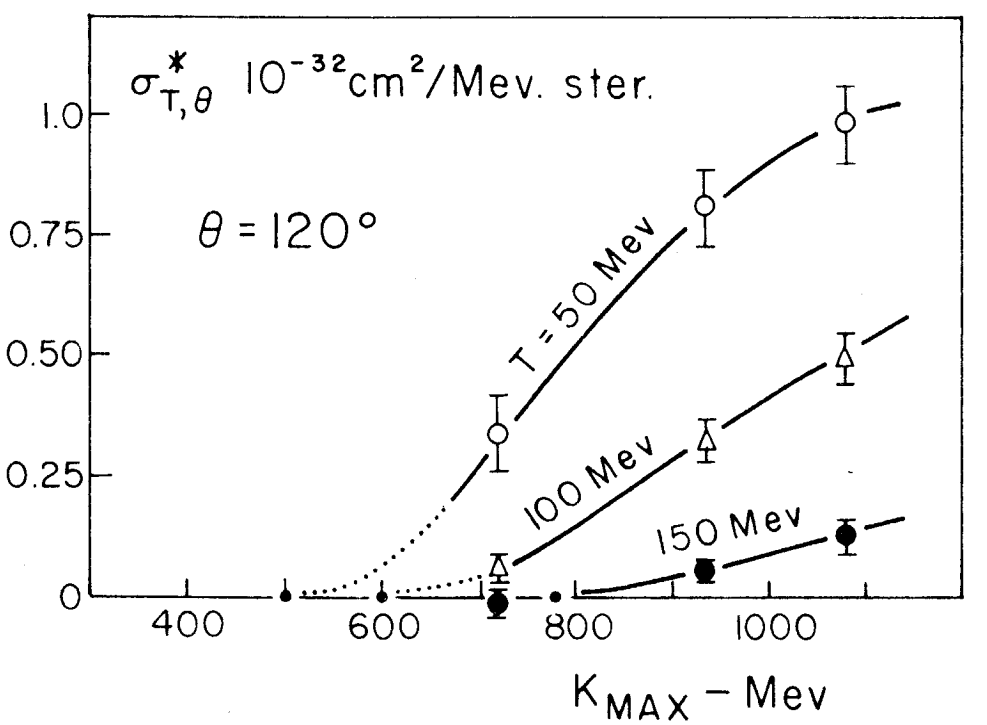
$\sigma^*_{T,\theta}$ 10^{-32}cm²/Mev. ster.
θ = 120°
T=50 Mev
100 Mev
150 Mev
1.0
0.75
0.50
0.25
0
400
600
800
1000
K_{MAX} – Mev

Figure 13. Comparison of the Data Obtained at Stanford University, Cornell University and the California Institute of Technology.

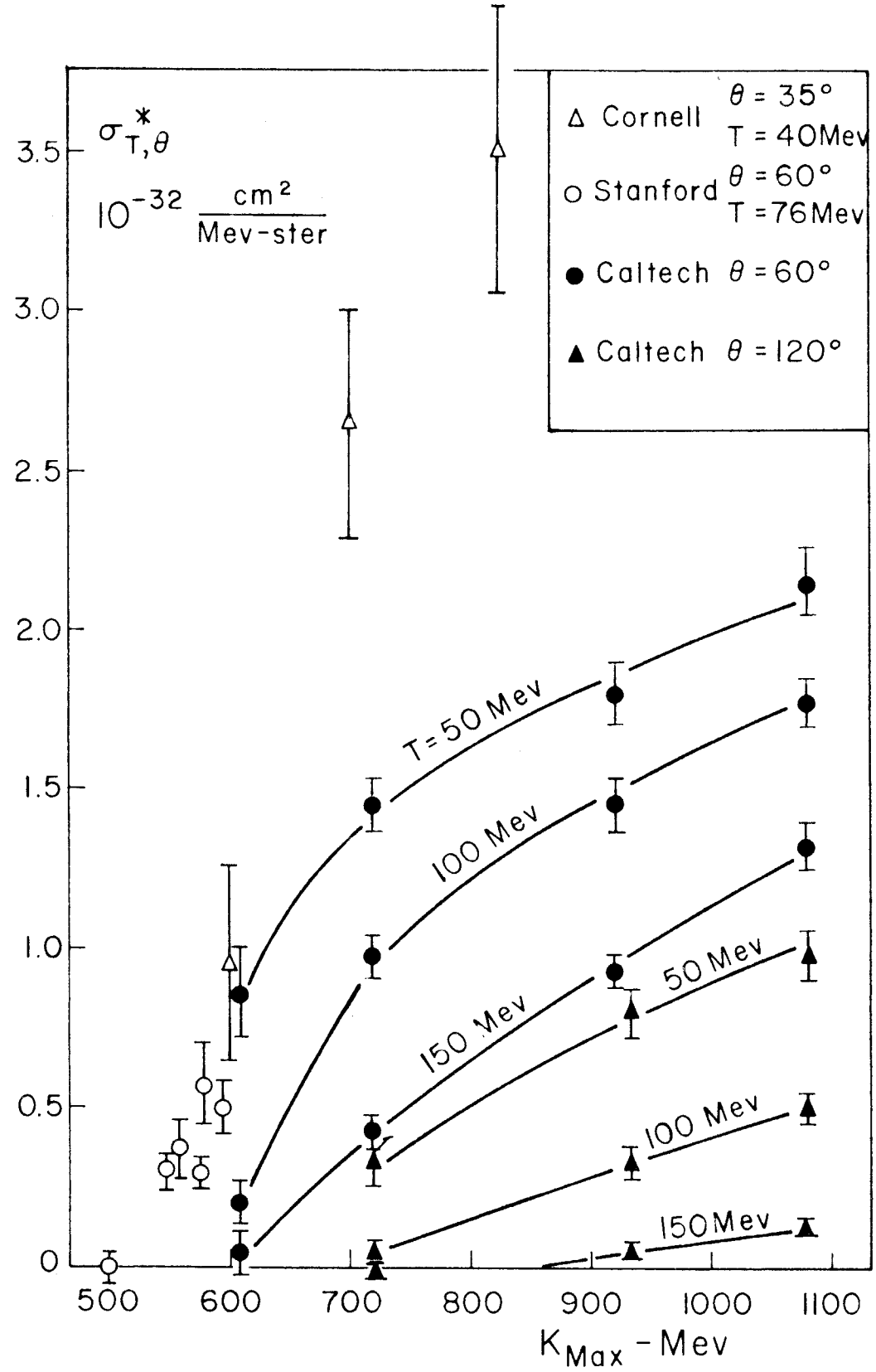
$\sigma^*_{T,\theta}$
10^{-32} $\frac{cm^2}{Mev\text{-}ster}$
Δ Cornell θ = 35° T = 40Mev
○ Stanford θ = 60° T = 76Mev
● Caltech θ = 60°
▲ Caltech θ = 120°
T = 50 Mev
100 Mev
150 Mev
50 Mev
100 Mev
150 Mev
3.5
3.0
2.5
2.0
1.5
1.0
0.5
0
500
600
700
800
900
1000
1100
K_{Max} - Mev

Figure 14a. Yields of Positive Pions Obtained at a Laboratory Angle of 60^{o}.

Figure 14b. Yields of Positive Pions Obtained at a Laboratory Angle of 120^{o}.

In both figures the dotted lines represent the contribution to the yields of single pion photoproduction.

a)

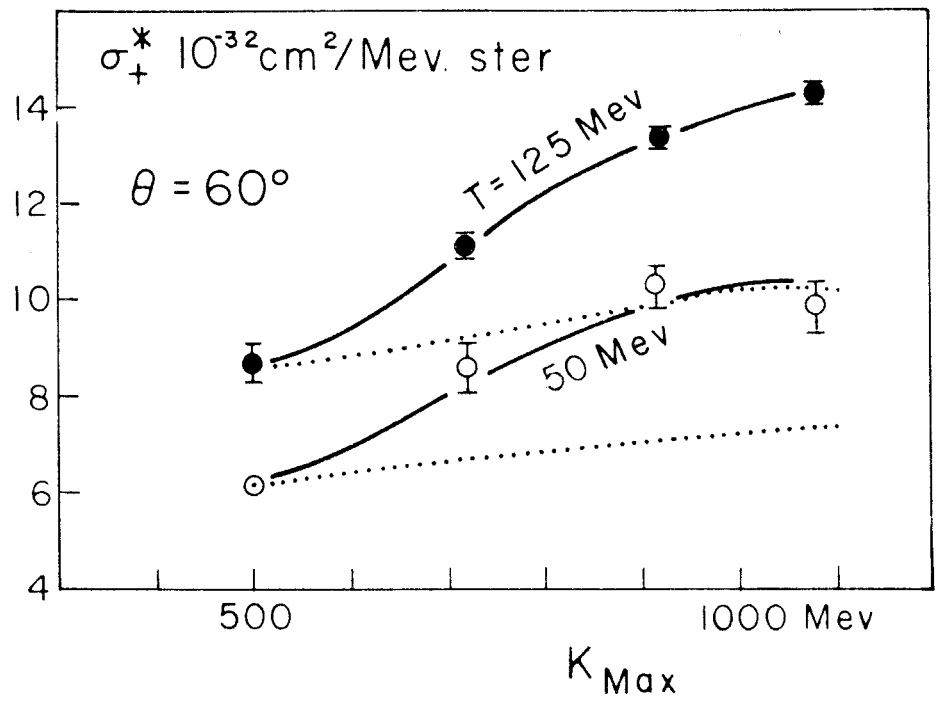
σ_+^* 10^{-32}cm^2/Mev. ster
θ = 60°
T = 125 Mev
50 Mev
14
12
10
8
6
4
500
1000 Mev
K_{Max}

b)

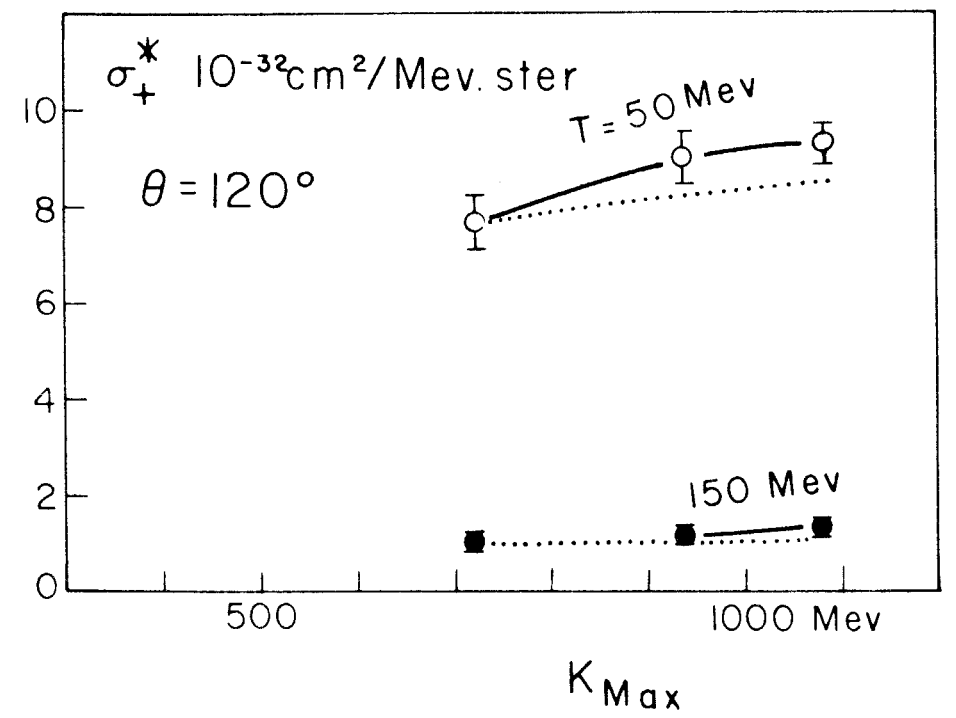
σ_+^* 10^{-32}cm^2/Mev. ster
θ = 120°
T = 50 Mev
150 Mev
10
8
6
4
2
0
500
1000 Mev
K_{Max}

a positive pion of energy T at an angle θ and E_o is the bremsstrahlung cut-off energy. As can be seen from figure 11a $B(E_o, k)$ increases slowly when E_o is increased. The increase in the yields due to single photoproduction can be computed easily and is represented by the dotted curves in figure 14. An estimate of the multiple production can then be obtained by comparing the experimental yields "per equivalent quantum" to the computed contribution of single photoproduction. Since no experimental data below the pair production threshold were taken at 60^o for 50 Mev pions, the corresponding contribution from single photoproduction was calculated from the cross-section obtained in a previous experiment (21). Within the rather large statistical errors the results are consistent with positive pion yields from multiple production about twice the corresponding negative pion yields. This is to be expected if the contribution of (π^+, π^-) and (π^+, π^o) pairs are equal.

B. Discussion of the Cross-Sections

The differential cross-sections, in the center of momentum system, for the photoproduction of negative pion in hydrogen are plotted as functions of the pion kinetic energy in figures 15, 16 and 17. The photon energies are approximately 660, 820 and 1000 Mev respectively. The data obtained at laboratory angles of 60^o and 120^o have been plotted in the same figure, the values of the angle of emission in the C.M. system being indicated above each experimental points. The dotted curves in figures 15 to 17 will be explained in the next section. (The values of the cross-sections in the laboratory system can be found in Tables VII and VIII).

Figure 15. Differential Cross-Sections, in the C.M. System, for the Photoproduction of Negative Pions in Hydrogen. Photon Energy k = 660 Mev.

Figure 16. Cross-Sections in the C.M. System for k = 820 Mev.

Figure 17. Cross-Sections in the C.M. System for k = 1000 Mev.

The arrows indicate the maximum pion energy allowable from pair production kinematics.

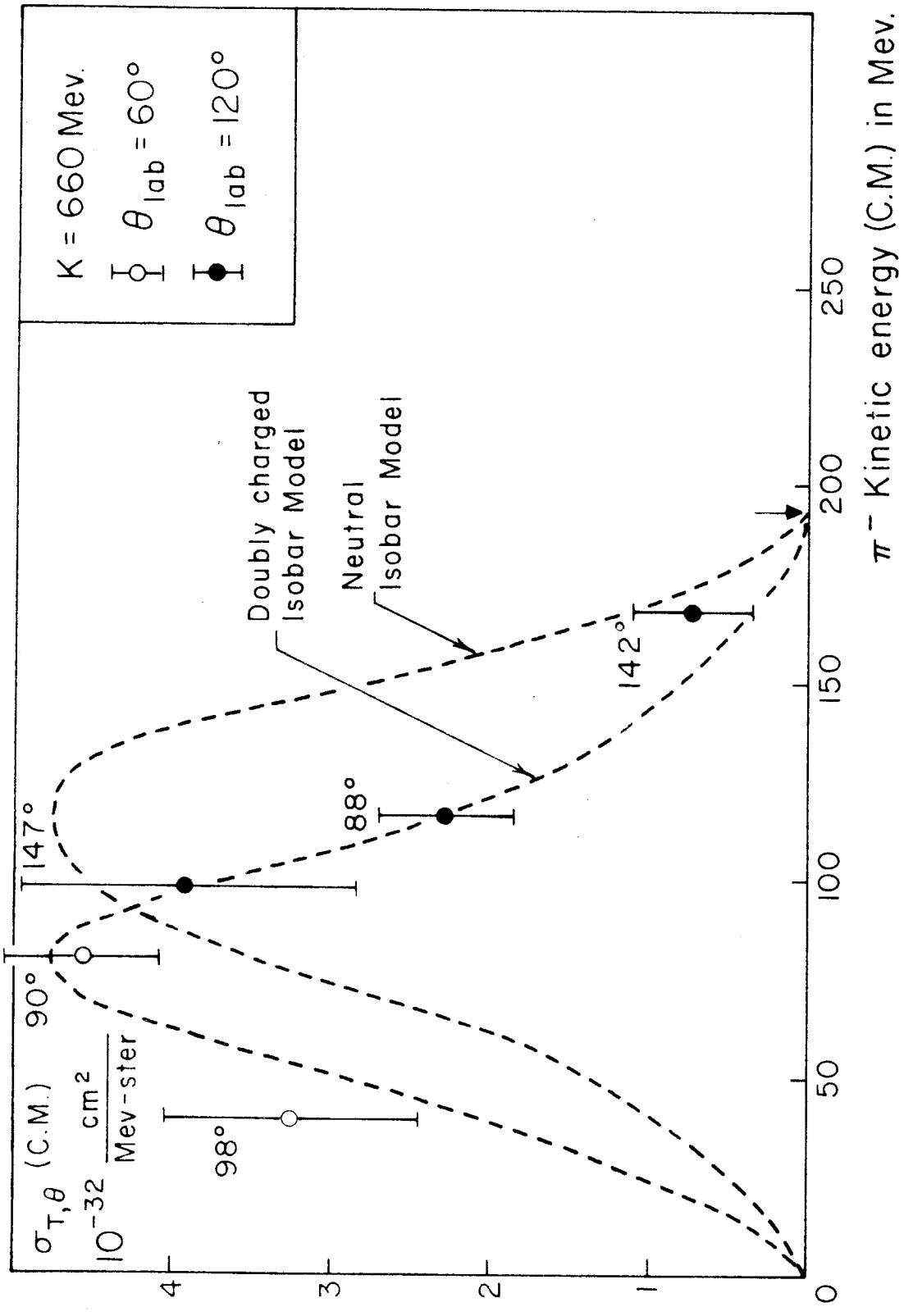
K = 660 Mev.
θ lab = 60°
θ lab = 120°
Doubly charged Isobar Model
Neutral Isobar Model
147°
88°
142°
98°
90°
σ T,θ (C.M.)
10^-32 cm^2 / Mev-ster
0
50
100
150
200
250
1
2
3
4
π⁻ Kinetic energy (C.M.) in Mev.

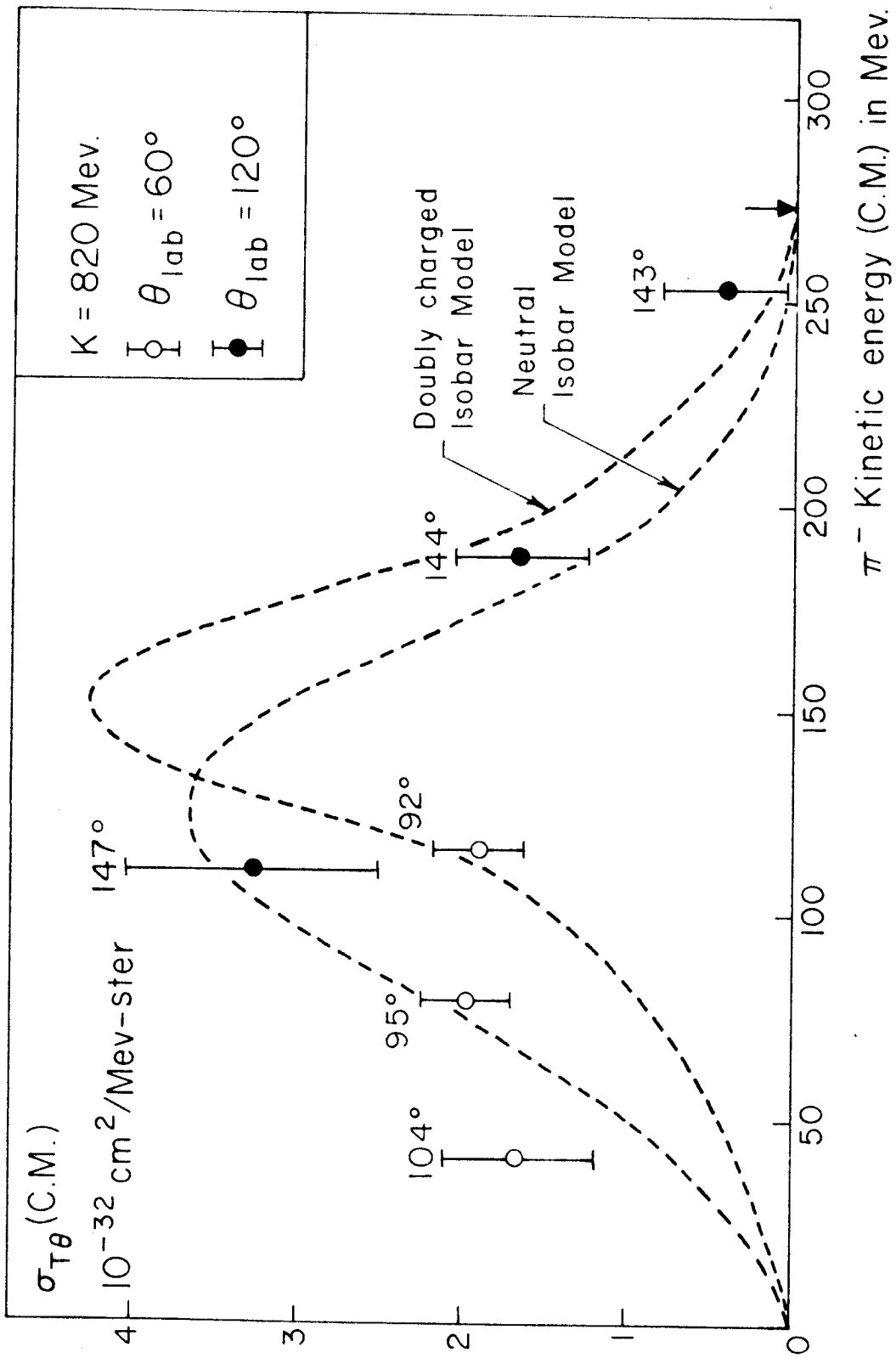
K = 820 Mev.
θ lab = 60°
θ lab = 120°
Doubly charged Isobar Model
Neutral Isobar Model
147°
144°
143°
104°
95°
92°
σTθ (C.M.)
10⁻³² cm²/Mev-ster
0
1
2
3
4
50
100
150
200
250
300
π⁻ Kinetic energy (C.M.) in Mev.

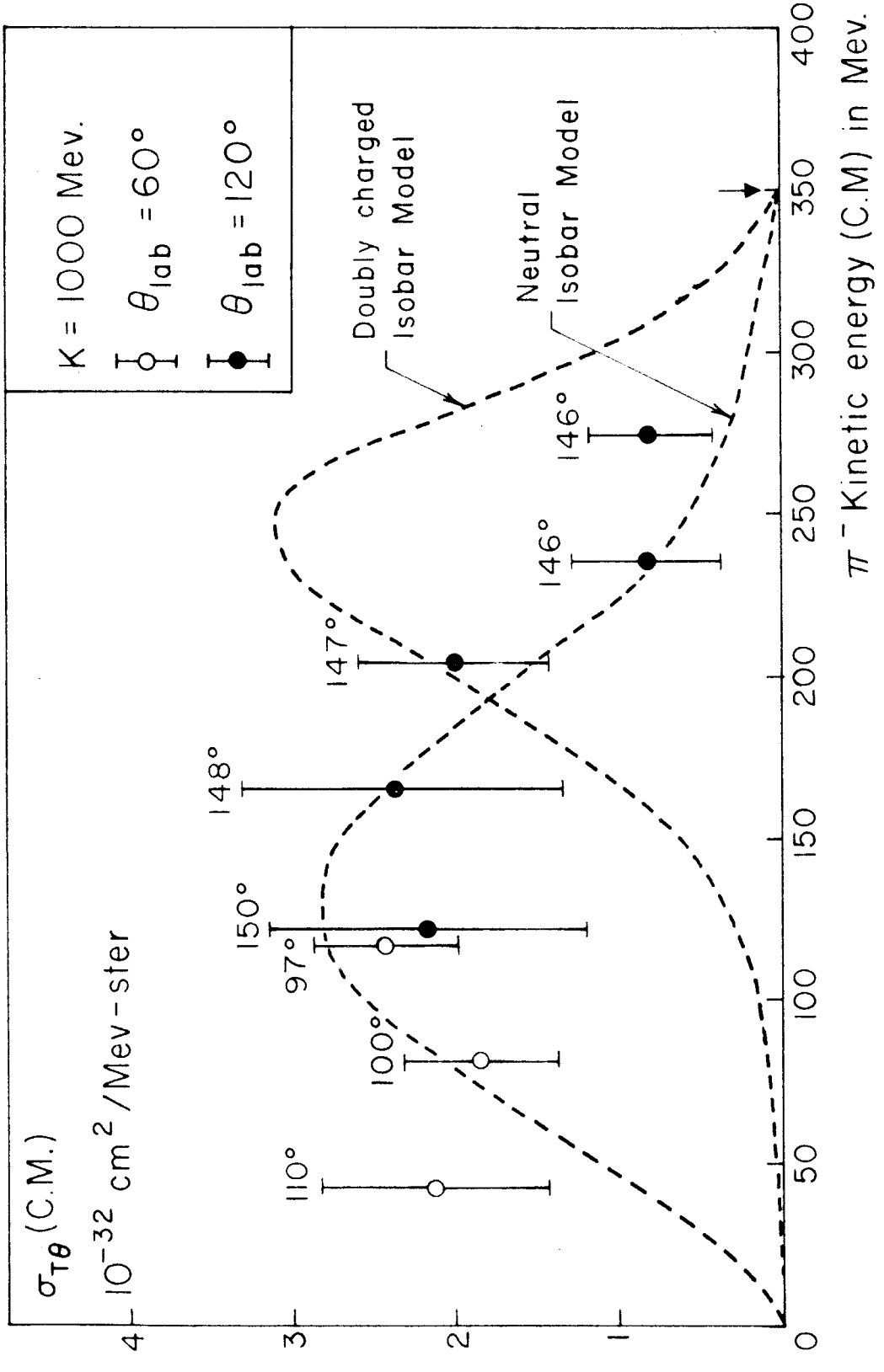
K = 1000 Mev.
θlab = 60°
θlab = 120°
Doubly charged Isobar Model
Neutral Isobar Model
146°
146°
147°
148°
150°
97°
100°
110°
σTθ (C.M.)
10⁻³² cm² /Mev-ster
π⁻ Kinetic energy (C.M) in Mev.
0
50
100
150
200
250
300
350
400
1
2
3
4

Two conclusions may be drawn from the plots of the cross-sections:

1. Angular Distribution

There is no evidence of a large angular anisotropy between the angles of 100° and 150° in the C.M. system. The values of the cross-sections at a kinetic energy of about 110 Mev at those two angles are the same within statistical errors at photon energies of 660 and 1000 Mev and only slightly outside the statistical errors at 820 Mev. In addition, all the experimental points at a given photon energy lie along a fairly smooth curve.

2. Total Cross-Sections

If at a given photon energy, the data obtained at laboratory angles of 60° and 120° are combined, then we have information on the cross-section in about the full range of pion energy allowed from the kinematics of the reaction. It is possible to integrate over the pion energy and obtain a cross-section per unit solid angle $\sigma_{\theta}(k)$. If we stretch our evidence somewhat further and assume that the pions are emitted isotopically in the C.M. system, then an estimate of the total cross-section for producing a negative pion in hydrogen can be obtained: $\sigma(k) = 4\pi\, \sigma_{\theta}(k)$.

In figure 18, the experimental results for the three photon energies studied have been plotted together. (To avoid confusion, curves representing good fits of the data replace the experimental points of figures 15 to 17). The result of the integration over pion energy is indicated in the figure.

Figure 18. Comparison of the Cross-Sections, in the C.M. System, Obtained at Three Photon Energies.

The result of the integration over pion energy is indicated in the figure.

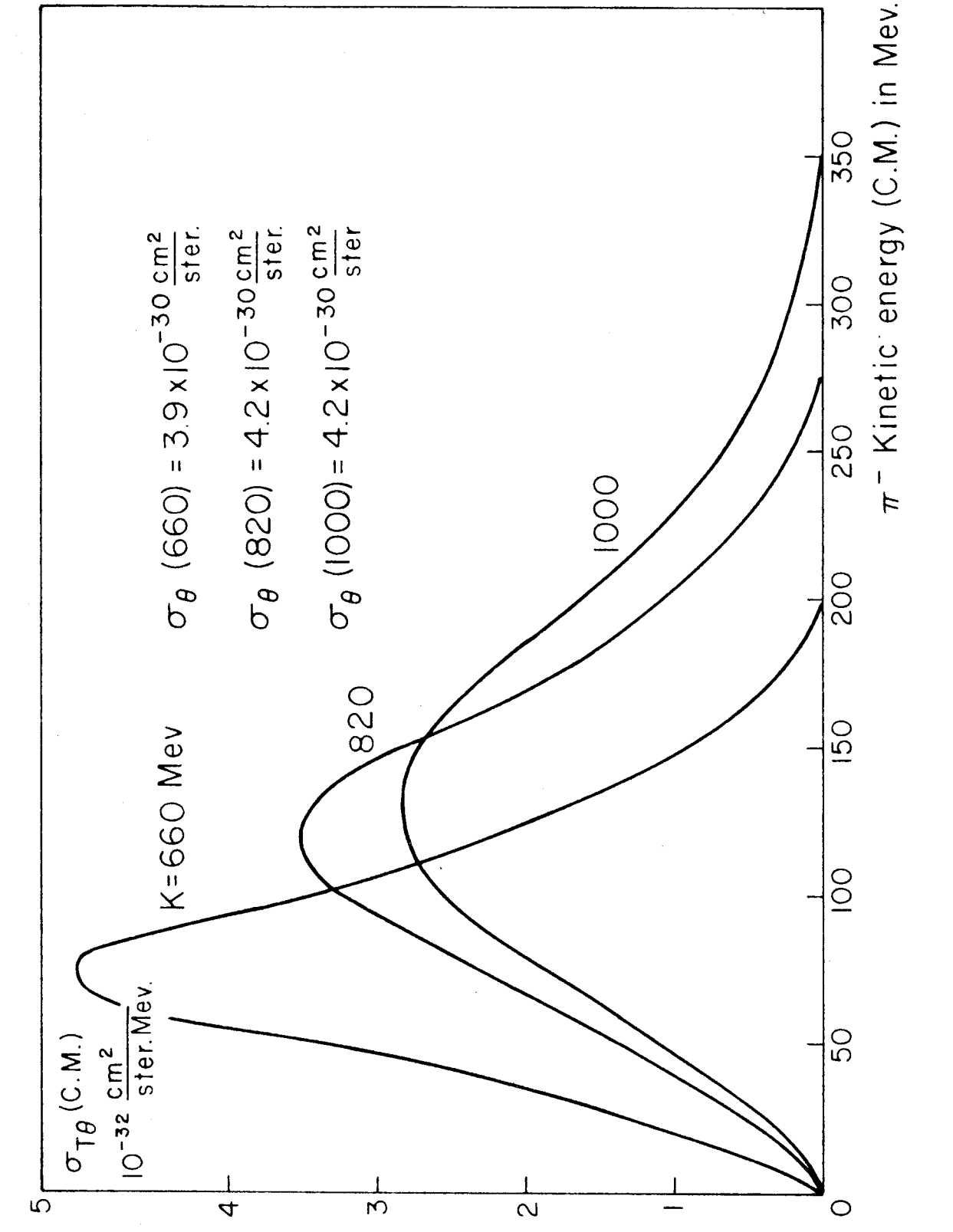
$\sigma_{T\theta}$ (C.M.)
10^{-32} $\frac{cm^2}{ster.Mev.}$
K=660 Mev
σ_θ (660) = 3.9×10^{-30} $\frac{cm^2}{ster.}$
σ_θ (820) = 4.2×10^{-30} $\frac{cm^2}{ster.}$
σ_θ (1000) = 4.2×10^{-30} $\frac{cm^2}{ster}$
820
1000
0
1
2
3
4
5
50
100
150
200
250
300
350
π^- Kinetic energy (C.M.) in Mev.

The curves representing "fits" of the data can be varied somewhat because of the large statistical errors on the experimental points and the result of the integrations may be in error by about 25 °/o. Within that uncertainty, the differential cross-section in the C. M. system is consistent with a constant value of about 4×10^{-30} cm^2/ster for all photon energies from 600 to 1100 Mev. The total cross-section if pion isotropy is confirmed, will be about 5×10^{-29} cm^2 in the same range of energy. It is interesting to note that the total cross-section for single production of neutral pions in hydrogen as measured in this laboratory (22, 23) is about $3.5 \times 10^{-29} cm^2$ in this range of photon energy. The cross-sections for single production of charged pions in hydrogen have not yet been measured but if they are not larger than the cross-sections for single production of neutral pions, then single and multiple pion production will occur with comparable probabilities in the interaction of photons in the 600 - 1100 Mev interval with the proton. The total cross-section for K-meson photoproduction is about 3×10^{-30} cm^2 (24) for 1 Gev photons.

C. Interpretation Attempts

1. Cutkosky - Zachariasen Calculation

The static cut-off theory of Chew and Low (2) was used by Cutkosky and Zachariasen (7) to calculate the photoproduction cross-sections of pion pairs in hydrogen. Unfortunately, their results are valid only for photon energies close to the threshold of the reaction for two main reasons.

(1) The assumption of a static nucleon (or M = ∞) enters in their calculations in many different respects (form of the interaction, kinematics, density of states, rejection of the states with two mesons in s-states etc.). However, for a photon energy of 1 Gev the velocity of the proton in the C.M. system is close to 0.5 c. Recently some relativistic methods of calculation have been developed (25) but have not been applied yet to the pair production problem.

(2) A specific assumption was made by Cutkosky and Zachariasen that one of the mesons is in an s-state and the other in a p-state. (Two mesons in a s-state can be obtained only with nucleon recoil and this is ruled out by the static nucleon assumption). There is no reason to believe this assumption to be valid at high energy, and in particular the case where both pions are in a p-state might even be preponderant if enough energy were available.

Because of their limitations the Cutkosky - Zachariasen calculations are compared only to our lowest energy data (k = 600 Mev). The theoretical predictions are plotted in figure 19 along with the experimental points. There is general agreement with respect to the magnitude of the cross-sections. The pion energy spectrum predicted does not agree too well with the experimental results. It must be pointed out that the C.M. system is not equivalent to the system of reference in which the proton has an infinite mass. In particular, the reaction thresholds are slightly different in the two systems. No corrections have been made on that account in the plot shown in figure 19.

Figure 19. Comparison of the Experimental Cross-Sections Obtained at k = 660 Mev to the Predictions of Cutkosky and Zachariasen.

The calculations were performed assuming a proton of infinite mass and a photon energy of k_o = 490 Mev. In the static-nucleon system the maximum pion energy is 210 Mev. On the other hand a photon having an energy of 660 Mev in the laboratory system will provide 518 Mev of available energy in the C.M. system. The corresponding maximum pion energy in the C.M. system will be 196 Mev.

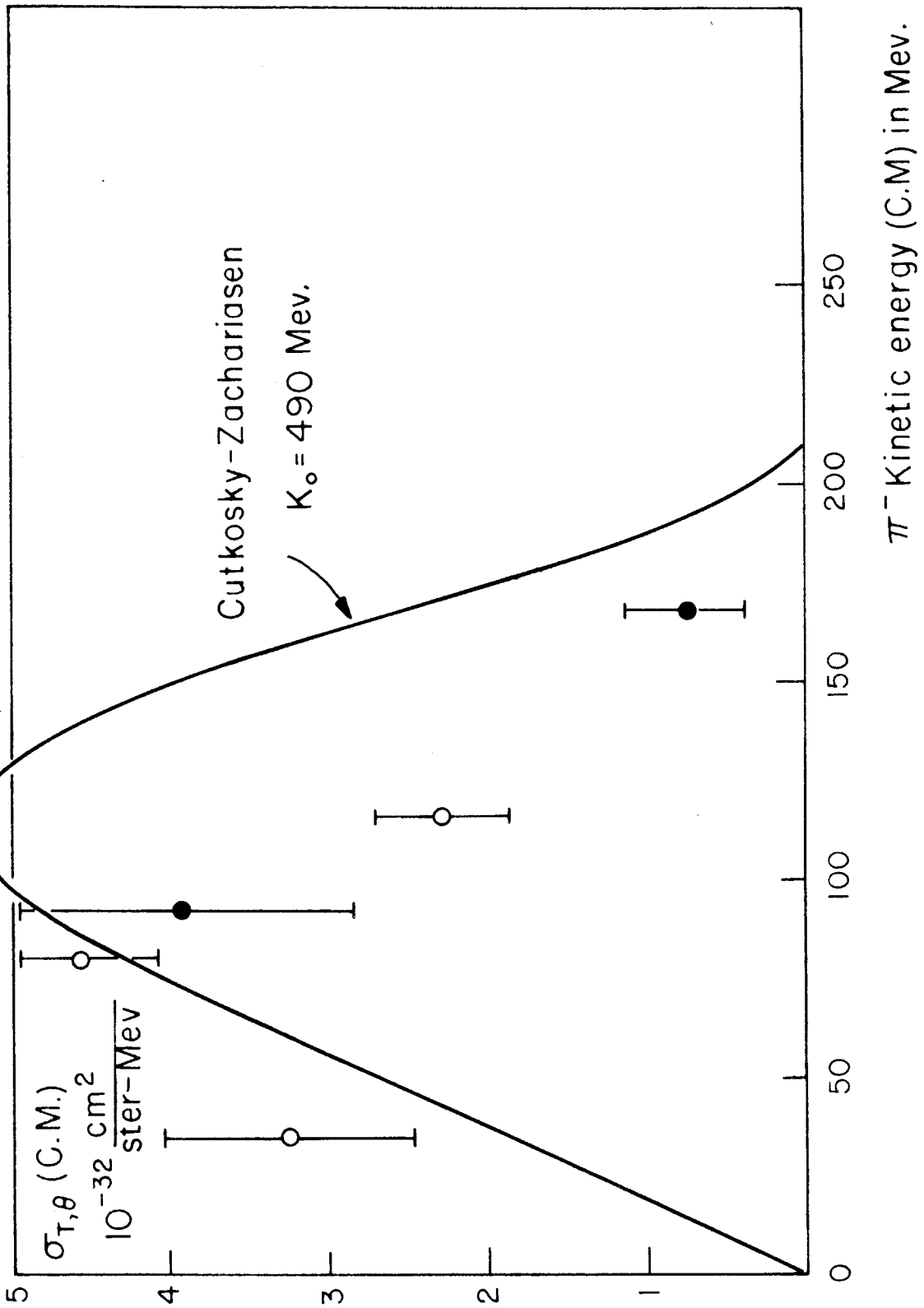
Cutkosky-Zachariasen
$K_o = 490$ Mev.
$\sigma_{T,\theta}$ (C.M.)
$10^{-32} \frac{cm^2}{ster-Mev}$
5
4
3
2
1
0
50
100
150
200
250
π^- Kinetic energy (C.M) in Mev.

2. Density of States

The energy spectrum of the negative pion produced by photons of a given energy is governed by the dependence on pion energy, of the matrix element of the interaction and by the corresponding density of states.

If it is assumed that the matrix element is independent of the pion energy, then a definite prediction of the pion energy spectrum is obtained. For a three particle final state the density of final states is given by:

$$\rho(E) = (2\pi)^{-6} \frac{E_3 E_2 p_2^3 p_1^2 \, dp_1 \, d\Omega_1 \, d\Omega_2}{p_2^2 (E - E_1) - E_2 \underline{p}_2 (\underline{p} - \underline{p}_1)}$$

where: E_i, p_i = energy and momentum of particle i (i = 1, 2, 3)

$E = \Sigma E_i$ $\underline{p} = \Sigma \underline{p}_i$ (in the C.M. system $\underline{p} = 0$)

$d\Omega_i$ = solid angle into which particle i comes out

$\hbar = c = 1$

Knowing the photon energy k one can calculate the energy available E, then $E_3 = E - E_1 - E_2$ and $\rho(E)$ is expressed as a function of two particles variables. However, since only one particle, the negative pion, is observed in our experiment an integration of the density of states over energy and angle of the second particle has to be performed. This integration has been made in the C.M. system for the three photon energies studied in this experiment (26). The results are plotted in

figure 20. A comparison with the experimental data in figures 15 to 17 shows that a fit with such pion energy spectra would be quite poor.

3. The Isobar Model

The idea that the 3/2, 3/2 resonant state of the pion nucleon system plays an important role in pion production has been applied with reasonable success to nucleon-nucleon and pion nucleon interactions (27, 28, 29). Several experiments have been performed at Brookhaven on the production of pions by pions (10, 11, 12) and have been interpreted in part, by a model in which one of the mesons stays with the nucleon in a short-lived excited state (isobar). Since the final state in the pion-production of pions, namely a nucleon and two mesons, is similar to the final state occurring in the photoproduction of pion pairs, it is possible that an isobar model might be successful in predicting the pion energy spectrum obtained in our experiment.

It is assumed that the probability for the formation of an isobar with a particular excitation energy Q is proportional to the product of two factors:

(1) The observed pion nucleon total scattering cross-section in the 3/2, 3/2 state at an incident pion kinetic energy in the C.M. system equals to Q. (The total scattering cross-section has a resonance for $Q \sim 150$ Mev with a width of about 100 Mev.)

(2) The two-body phase space factor ρ for the scattered pion and the isobar. Unfortunately no isotopic spin can be assigned to the photon and since we are observing only the negative pion, two reactions are possible :

Figure 20. Density of States for a Pion Pair Photoproduction.

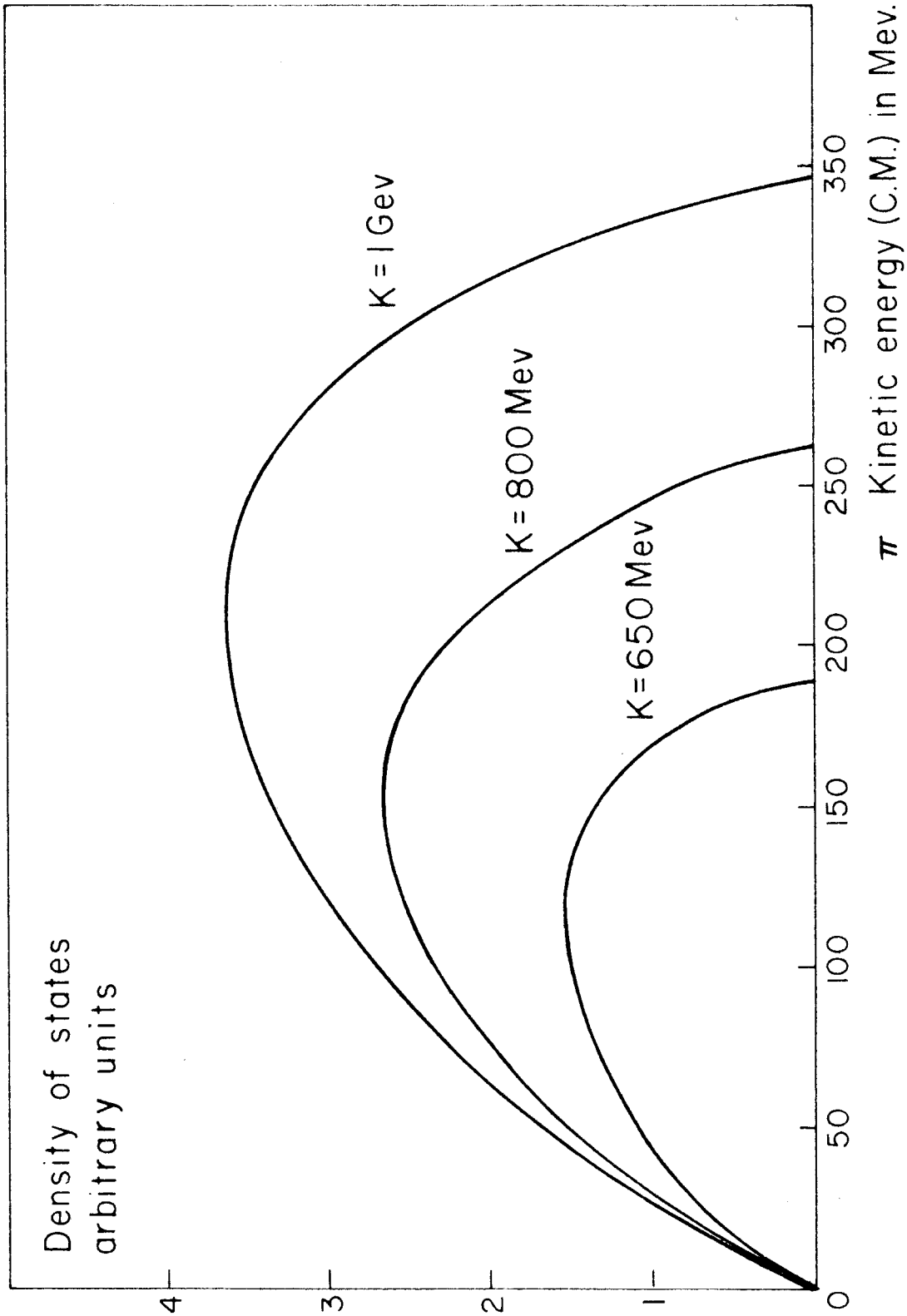
Density of states
arbitrary units
4
3
2
1
0
50
100
150
200
250
300
350
π Kinetic energy (C.M.) in Mev.
K = 1 Gev
K = 800 Mev
K = 650 Mev

$$\gamma + P \longrightarrow P^* + \pi^- \longrightarrow P + \pi^+ + \pi^- \quad \text{(doubly charged isobar)}$$

$$\gamma + P \longrightarrow P^* + \pi^+ \longrightarrow P + \pi^- + \pi^+ \quad \text{(neutral isobar)}$$

The z-component of the isotopic spin of the system is $\tau_z = 1/2$ from charge conservation but we do not know the total isotopic spin τ of the system. If it is assumed that the only possible values of τ are $\tau = \tau_z = 1/2$ and $\tau = \tau_z + 1 = 3/2$ and that the corresponding states occur with amplitudes α and β respectively, then it can be shown that the ratio $\alpha/\beta = 4/\sqrt{5}$ leads to a pure doubly charged isobar, and $\alpha/\beta = -2/\sqrt{5}$ to a pure neutral isobar. Since we do not possess any information on α/β, the two possible isobars will be examined separately.

a. Doubly Charged Isobar

If the reaction proceeds through the doubly charged isobar the energy spectrum of the negative pion is given simply by:

$$P(E)dE = A\, \rho(E)\, \sigma(Q)\, \frac{dQ}{dE}\, dE$$

where A is an undetermined constant. In the C. M. system:

$$\rho(E) = \frac{(E_o - E)\, E \sqrt{E^2 - m^2}}{E_o}$$

where E_o is the energy available in the C. M. system; m = pion rest mass. It can be shown easily from two-body reaction kinematics that:

$$Q = \sqrt{E_o^2 - 2E_oE + m^2} - (M + m)$$

$$dQ/dE = -E_o/(M + m + Q)$$

The resulting spectra are plotted in dotted line in figures 15 to 17, the constant A of the spectra being adjusted to fit the experimental points as well as possible for each photon energy.

b. Neutral Isobar

If the reaction proceeds through the neutral isobar the process is more complicated than the preceding one since the observed negative pion comes from the decay of the isobar itself. We make the additional a priori assumption that the positive pion is emitted in an s-state, hence that the isobar is produced isotopically in the C.M. system.

Call S (unprimed) the C.M. system, E^*, p^*, β^* etc. the isobar variables in this system, E, p, β etc. the negative pion variables. Call S' (primed) the isobar rest system, and E', p', etc. the negative pion variables in that system, θ' being the angle between the π^- momentum vector and the isobar velocity vector β^* in the system S'. If we assume that the isobar decays isotropically in its own system (S'), the probability distribution of the two variables Q and θ' will be:

$$P(Q, \theta')\, dQ\, d\theta' = A\, \rho(Q)\, \sigma(Q)\, dQ\, d(\cos\theta')$$

where as before $\rho(Q)$ is the two-body density of states for the creation of the isobar and $\sigma(Q)$ is the 3/2, 3/2 total pion-nucleon cross-section.

Now, the pion energy E is a function of Q and θ' only, $E = E(Q, \theta')$ and performing a change of variables:

$$P(E, Q)\, dE\, dQ = \frac{1}{\frac{\partial E}{\partial \cos\theta'}} \rho(Q)\, \sigma(Q)\, dQ\, dE$$

The pion energy spectrum is then given by:

$$P(E)\, dE = \int_{Q_{max}(E)}^{Q_{max}(E)} \rho(Q)\, \sigma(Q)\, \frac{\frac{dQ}{\partial E}}{\partial \cos\theta'}\, dE$$

where the limits of the integration are obtained from the condition $-1 < \cos\theta' < +1$.

From the Lorentz transformation:

$$E = E' \gamma^* (1 + \beta^* \beta' \cos\theta')$$

where

$$\gamma^* = (1 - \beta^{*2})^{-1/2}$$

we deduce immediately:

$$\frac{\partial E}{\partial \cos\theta'} = p' \beta^* \gamma^* .$$

The method of calculation to get P(E) is now straightforward.

(1) Given a photon energy calculate β^*, γ^*, E', β' as a function of Q.

(2) Plot $E_{max} = \gamma^* E' (1 + \beta^* \beta')$ and $E_{min} = \gamma^* E' (1 - \beta^* \beta')$.

(3) For a given E find $Q_{max}(E)$ and $Q_{min}(E)$.

(4) Finally perform the integration leading to P(E).

The resulting spectra, adjusted to fit the experimental data as well as possible are plotted with the experimental data in figures 15 to 17 (above).

It can be seen that, for photon energies of 820 Mev and 1000 Mev, the neutral isobar hypothesis gives a good fit to the experimental data and that the doubly charged isobar hypothesis does not. The situation is reversed for a photon energy of 660 Mev where the doubly charged isobar model gives the best fit to the experimental data.

VI. CONCLUSION

The multiple production of pions in the interaction of γ-rays with protons has been studied by observing the negative pions emitted in that interaction. Cross-sections have been obtained for photon energies up to 1 Gev at laboratory angles of 60° and 120°. When the cross-sections are expressed in the C. M. system, they do not show a large angular dependence. If the negative pions are indeed emitted nearly isotropically in the C. M. system, then the total cross-sections for π^- photoproduction in hydrogen are consistent with a constant value of about $5 \times 10^{-29} cm^2$. The observed pion energy spectra can be fitted fairly well with the predictions of the "isobar model". Since negative pions alone are observed, the "isobar" can have two charge states; one of them (neutral) fits the data at a photon energy of 820 Mev and 1 Gev, the other one (doubly charged) fitting the data somewhat better at 660 Mev.

The results of this experiment suggest several directions of future investigations. The angular distribution of the negative pions should be studied more extensively. At a smaller laboratory angle the maximum energy of a pion emitted from a reaction caused by a 1 Gev photon may reach several hundreds of Mev and a larger spectrometer will have to be used.

The switch-over of the two isobar models to fit the data when the incident photon energy is increased, is puzzling. The models may not have any physical significance but since they give definite predictions also for the energy spectrum of the pair-produced positive pions, a check on the models is possible. The easiest way to obtain data on the

positive pion may be through the detection of both π^+ and π^- in coincidence.

An estimate of the number of proton recoils from a multiple photoproduction has been made in connection with an experiment performed to measure the neutral pion photoproduction in hydrogen (22). That estimate, together with our results, indicate that the (π^o, π^o) pair contribution might be much smaller than the (π^+, π^-) contribution. This result is to be expected near the threshold of the pair reaction* but is somewhat surprising at higher photon energy.

No information on the relative multiplicity of pions in photoproduction at high energy can be deduced safely from the results of this experiment. The success of the isobar model, if it is confirmed by further experiments, might be an indication that triple production is not too significant compared to pair production. On the other hand, the constancy of the total cross-section with photon energy and the fact that the pion energy spectra peak at low energy, could be indications of a significant triple production. That question will be more easily answered by bubble or cloud-chamber experiments one of which is already in progress (30).

Finally, it is hoped that the availability of the experimental results obtained in this work will spur the search for new developments in the theoretical interpretation of multiple pion photoproduction at high energy.

---

* In the static theory a π^o cannot be emitted in a s-state.

APPENDIX I.

CHANCE COINCIDENCES MONITORING

Consider three counters and denote the counting rates in each of them during a given run by $(1)^*$, $(2)^*$, $(3)^*$ respectively. These counting rates are produced by different types of events which we can separate into mutually exclusive independent events, namely:

(1): counting rate caused by particles crossing the counter 1 only, or by noise from the photomultipliers of the counter 1; similarly (2) and (3)

(12-3): counting rate caused by particles crossing counters 1 and 2 but missing the counter 3; similarly (13-2) and (23-1)

(123): counting rate caused by particles crossing all three counters.

We can write:

$$(1)^* = (1) + (12\text{-}3) + (13\text{-}2) + (123) \tag{1}$$

$$(2)^* = (2) + (12\text{-}3) + (23\text{-}1) + (123) \tag{2}$$

$$(3)^* = (3) + (13\text{-}2) + (23\text{-}1) + (123) \tag{3}$$

Then the counting rate of two-fold coincidences is:

$$(12)^* = (12\text{-}3) + (123) + \Big[(1) + (13\text{-}2)\Big]\Big[(2) + (23\text{-}1)\Big]\, 2\tau \tag{4}$$

where τ is the resolving time of the coincidence circuit. The last term in equation 4 represents the chance double coincidences rate.

We assume that all rates are proportional to the beam intensity B(t) (B(t) is in units of bips/sec for example). If we call $[1]$ the

number of counts from particles crossing counter 1 only in a run of duration T then:

$$[1] = \frac{(1)}{B(t)} \int_0^T B(t)\, dt = (1)\, \frac{B^{(1)}\, T}{B(t)} \qquad (5)$$

where

$$B^{(1)} = \frac{1}{T} \int_0^T B(t)\, dt = \text{time average of } B(t) \text{ during the run} \qquad (6)$$

Similar relations, can be obtained for $[12\text{-}3]$, $[123]$ etc. Substituting the values of (1), (12-3) etc. from equation 5 into equation 4, the observed number of two-fold coincidences in a run of duration T will be

$$[12]^* = [12\text{-}3] + [123] + \left\{[1] + [13\text{-}2]\right\}\left\{[2] + [23\text{-}1]\right\} \frac{2\tau}{T} \frac{B^{(2)}}{(B^{(1)})^2} \qquad (7)$$

where

$$B^{(2)} = \frac{1}{T} \int_0^T B^2(t)\, dt = \text{time average of } B^2(t) \text{ during the run} \qquad (8)$$

(note that for a "1 bip" run $B^{(1)}\, T = 1$).

Similar considerations lead to the number of accidental triple coincidences in a run of duration T .

$$[A] = [123]^{*} - [123] = \left[\left\{[1] + [12-3]\right\}[23-1] + \left\{[2] + [23-1]\right\}[13-2] + \left\{[3] + [13-2]\right\}[12-3]\right] \frac{2\tau}{T} \frac{B^{(2)}}{(B^{(1)})^2} + [1][2][3] \frac{4\tau^2}{T^2} \frac{B^{(3)}}{(B^{(1)})^3} \quad (9)$$

where

$$B^{(3)} = \frac{1}{T}\int_0^T B^3(t)\,dt = \text{time average of } B^3(t) \text{ during the run} \quad (10)$$

The accidental monitor counts the delayed coincidences between two-fold coincidences between pulses from counters 1 and 2 and pulses from counter 3. The counting rate (M) for the monitor is:

$$(M) = (12)^{*}\,(3)^{*}\,2\tau \quad (11)$$

Since the events leading to $(12)^{*}$ and $(3)^{*}$ are independent because of the delay, the indication of the monitor in a run of duration T is found to be:

$$[M] = \left\{[12-3] + [123]\right\}\left\{[3] + [13-2] + [23-1] + [123]\right\} \frac{2\tau}{T} \frac{B^{(2)}}{(B^{(1)})^2} + \left\{[1] + [13-2]\right\}\left\{[2] + [23-1]\right\}\left\{[3] + [13-2] + [23-1] + [123]\right\} \frac{4\tau^2}{T^2} \frac{B^{(3)}}{(B^{(1)})^3} \quad (12)$$

A comparison between equations 9 and 12 indicates that the relationship between the actual number of chance coincidences and the

indication of the monitor is quite complicated. Besides, since the beam dump is unpredictable, no accurate value of $B^{(2)}$ and $B^{(3)}$ can be obtained.

Equations 9 and 12 are considerably simplified by the use of the inequalities:

$$\begin{matrix}(1) \\ (2) \\ (3)\end{matrix} \quad \begin{matrix}(12\text{-}3) \\ (13\text{-}2) \\ (23\text{-}1)\end{matrix} \gg (123)$$

(see the numerical values next section). Then

$$[A] \sim \left\{[1][23\text{-}1] + [2][13\text{-}2] + [3][12\text{-}3]\right\} \frac{2\tau}{T} \frac{B^{(2)}}{(B^{(1)})^2} + [1][2][3] \frac{4\tau^2}{T^2} \frac{B^{(3)}}{(B^{(1)})^3} \qquad (9')$$

and

$$[M] \sim [3][12\text{-}3] \frac{2\tau}{T} \frac{B^{(2)}}{(B^{(1)})^2} + [1][2][3] \frac{4\tau^2}{T^2} \frac{B^{(3)}}{(B^{(1)})^3} \qquad (12')$$

A. Application to the Experiment

The quantities $[1]$, $[12\text{-}3]$, $[123]$ etc. can be obtained experimentally by running the machine with a low intensity beam. The chance coincidences are then negligible and $[1] \sim [1]^*$, $[12\text{-}3] \sim [12]^*$ etc. We found:

$$[1] \sim 1.4\,[2] \sim 1.4\,[3] \sim 2000 \text{ counts per bip}$$

$[12\text{-}3] \sim 3$ $[13\text{-}2] \sim 1.5$ $[23\text{-}1] \sim 40$ counts per bip

$[123] \sim 1$ to 4 counts per bip for negative pion runs.

Assume a constant beam intensity B_1 during the dump. From equations 9' and 12' and using the measured value of $2\tau = 5 \times 10^{-7}$ sec we get the relation between $[A]$ and $[M]$ "per bip"

$$[A] = [M]\left(1 + \frac{36}{28 + B_1}\right) \tag{13}$$

Let us consider two possible beam intensities.

a) Low beam intensity Some data were taken with an intensity as low as 50 bips an hour. Since the beam dump has a duration of 20 m sec, that beam intensity corresponds to $B_1 = 0.7$ then

$$[A] = 2.25\,[M]$$

b) High beam intensity The highest beam intensity achieved in this experiment was about 500 bips an hour corresponding to $B_1 = 7$. In this case

$$[A] = 2.0\,[M]$$

It was found experimentally that the indications of the accidentals monitor were only a few per cent of the total number of triple coincidences. We feel justified from the results above to use the approximate relation $[A] = 2\,[M]$ in the analysis of the data.

APPENDIX II.

CORRECTION FOR DECAY OF PIONS IN FLIGHT

The distance between target and counters in the magnetic spectrometer is long enough, so that the pion have an appreciable probability of decaying before reaching the counters. From the knowledge of the pion mean life-time, it is easy to calculate the fraction R_π, of the pions which arrive at the counters before decay. This fraction must however be corrected upward for those pions whose decay muons are registered by the counter system. An additional correction must be made for those decay muons originating from pions which would not have been counted because they have either the wrong energy of the wrong direction of emission from the target.

Call C_π and C_μ the observed counting rates due to pions and muons. C_o the counting rate which would be found if no decay occurred. The decay correction, $R = (C_\pi + C_\mu)/C_o$, may be calculated as follows. Let S be the total length along the path of the central ray from target to counter. Distances along this central ray will be measured from the target as origin and labeled s. If the mean life of the pion is τ , then the free mean path for decay is:

$$\lambda = p\tau/m \qquad (1)$$

and

$$R_\pi = C_\pi/C_o = e^{-S/\lambda_o} \qquad (2)$$

where $\lambda_o = p_o\tau/m$, p_o being the momentum selected by the spectrometer

and m being the rest mass of the pion.

If $c_\mu(s)\,ds$ is the counting rate of muons which originate at s (within ds) from the decay of a pion of momentum p, then

$$C_\mu = \int_o^S c_\mu(s)\,ds$$

It is convenient to express $c_\mu(s)$ in terms of the number of pions which decay in ds, but which would have been selected by the spectrometer had they not decayed. This number is:

$$c_o(s)\,ds = C_o e^{-s/\lambda_o}\,ds/\lambda_o$$

Call $f(s) = c_\mu(s)/c_o(s)$ then:

$$C_\mu = C_o \int_o^S f(s)\, e^{-s/\lambda_o}\,ds/\lambda_o \qquad (3)$$

and

$$R = (C_\pi + C_\mu)/C_o = e^{-S/\lambda_o} + \int_o^S f(s)\, e^{-s/\lambda_o}\,ds/\lambda_o \qquad (4)$$

The calculation of f(s) is made in a different way for mesons which decay before reaching the magnet than for those decaying after the magnet so the two regions will be discussed separately.

A. Decays Before the Magnet Aperture

Assume a point source and call $Q(p_\pi)dp_\pi$ the number of pions per steradian with momentum p_π within dp_π. The number of pions in

this momentum range which decay at a distance s within the volume element $rdrd\varphi ds$ of figure A1 is:

$$Q(p_\pi)dp_\pi e^{-s/\lambda} \frac{ds}{\lambda} \quad \frac{rdrd\varphi}{s^2} \tag{5}$$

where

$$\lambda = \tau p_\pi / m$$

The probability that the muon from these decays crosses the element of area $d\xi\, d\eta$ of the magnet entrance aperture can be called

$$P(p_\pi, \alpha) \quad \frac{d\xi\, d\eta}{(L-s)^2}$$

where α is the angle between the directions of the muon and the incident pion and is defined when s, r, φ, ξ and η have been chosen. The condition that the muon be counted, determines a region in the $r\varphi$ plane for given p, s, ξ and η. Outside that region, the decay muon misses the counters.

The muon counting rate from decays at s is:

$$c_\mu(s)ds = e^{-s/\lambda} \frac{ds}{\lambda} \iint Q(p_\pi)dp_\pi \quad \frac{rdrd\varphi}{s^2} \; P(p_\pi, \alpha) \; \frac{d\xi\, d\eta}{(L-s)^2} \tag{6}$$

The $d\xi\, d\eta$ integral is over the magnet entrance aperture. The $drd\varphi$ integral is limited by the lead shielding walls and by the region at s from which muons from pions of momentum p_π pass through the counters.

Figure A1. Schematic View of the Spectrometer Illustrating the Parameters used in the Calculation.

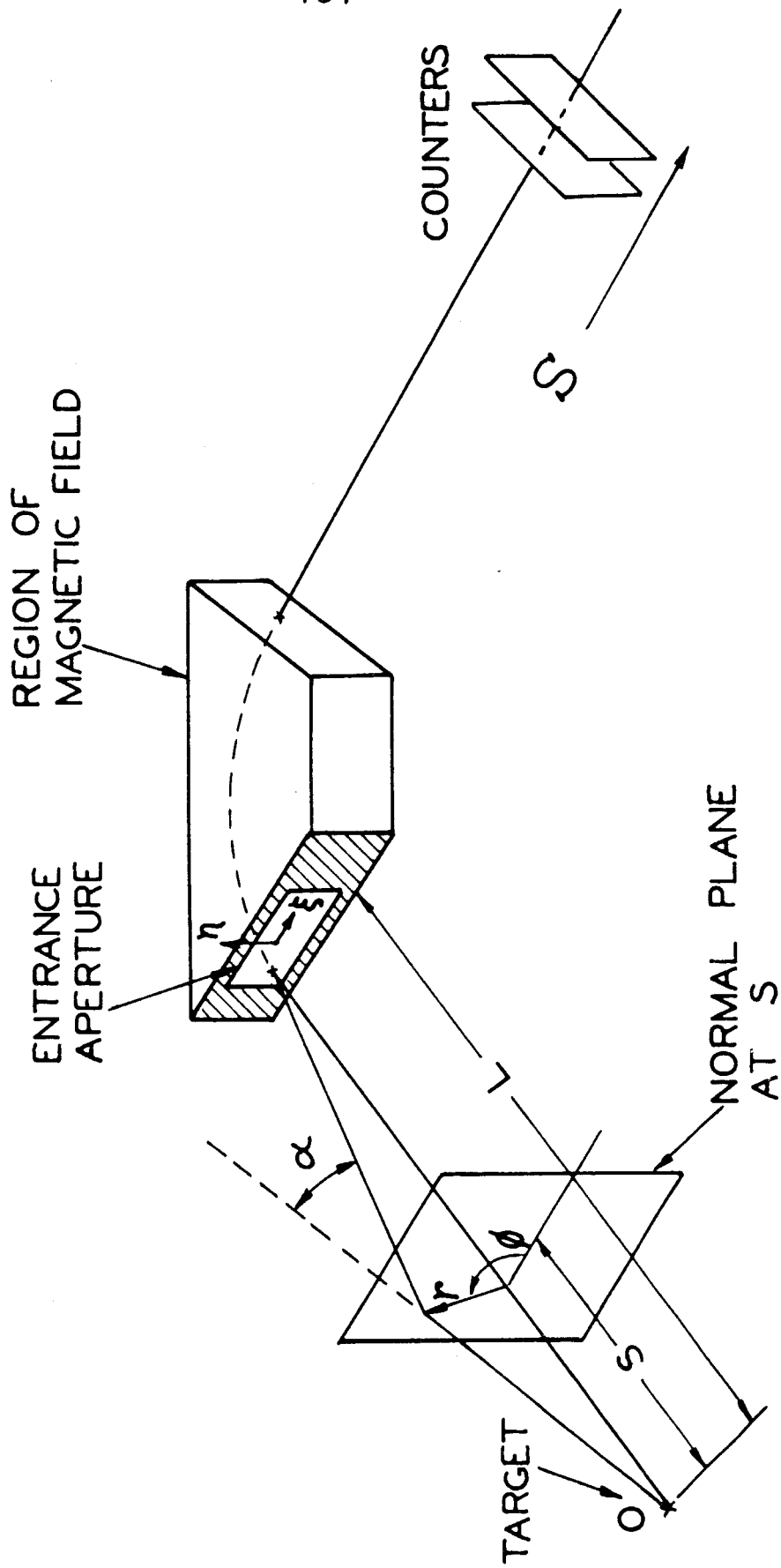
COUNTERS
S
REGION OF
MAGNETIC FIELD
ENTRANCE
APERTURE
η
ξ
α
l
NORMAL PLANE
AT S
r
φ
s
TARGET
O

Now,

$$c_o(s)ds = Q(p_o)\Delta p_o\, \Delta\Omega\, e^{-s/\lambda_o}\, ds/\lambda_o \qquad (7)$$

where Δp_o and $\Delta\Omega$ are determined by the spectrometer characteristics. Hence:

$$f(s) = \frac{c_\mu(s)}{c_o(s)} = \frac{e^{-s/\lambda}}{e^{-s/\lambda_o}} \frac{\lambda_o}{\lambda} \iiint \frac{Q(p_\pi)dp_\pi}{Q(p_o)\Delta p_o} P(p_\pi,\alpha) \frac{r\,dr\,d\varphi\,d\xi\,d\eta}{\Delta\Omega s^2(L-s)^2}$$

The momentum spectrum $Q(p_\pi)$ of the pion depends on the reaction which produces them. Since we want to obtain an expression which can be used to calculate the π-μ decay correction for any reaction, we can write:

$$R_\mu(p_o)(\text{before magnet}) = \frac{C_\mu(\text{before magnet})}{C_o} = \int g(p_\pi, p_o) \frac{Q(p_\pi)}{Q(p_o)}\, dp_\pi \qquad (8)$$

with

$$g(p_\pi, p_o) = \int \gamma(p_\pi, s)ds = \int e^{-s/\lambda} \frac{ds}{\lambda} \iiint P(p_\pi,\alpha) \frac{r\,dr\,d\varphi\,d\xi\,d\eta}{\Delta p_o \Delta\Omega s^2(L-s)^2} \qquad (9)$$

The computation of $\gamma(p_\pi, s)$ is, in general, a rather complicated numerical task; however, estimates made for another spectrometer (31) have shown that $\gamma(p_\pi, s)$ is a smooth function of s. There are two values of s (s = 0 and s = L) where $\gamma(p_\pi, s)$ can be calculated fairly

easily and we have used a linear interpolation between these two values to estimate $g(p_\pi, p_o)$.

1. Decay at the Source: s=0.

Since the muons originate at the source, they are counted if their momentum is p_o within Δp_o. Now, it is easy to show that $\alpha \sim \frac{L\ r}{s(L-s)}$ (see figure A2) so that $\frac{r dr}{s^2(L-s)^2} = \frac{\alpha\, d\alpha}{L^2}$.

Substituting into equation 9

$$\gamma(p_\pi, s) = \frac{e^{-s/\lambda}}{\lambda} \iiint P(p_\pi, \alpha)\ \frac{\alpha\, d\alpha d\varphi d\xi d\eta}{\Delta p_o\, \Delta\Omega\, L^2} \qquad (10)$$

But, at s = 0, $\iint \frac{d\xi\, d\eta}{L^2} = \Delta\Omega$ and $\int d\varphi = 2\pi$.

Furthermore $P(p_\pi,\alpha)\ 2\pi \sin\alpha\, d\alpha \sim 2\pi P(p_\pi,\alpha)\alpha\, d\alpha = P(p_\pi, T_\mu)\, dT_\mu$

where dT_μ corresponds to $d\alpha$ and $P(p_\pi, T_\mu)\, dT_\mu$ is the probability that a pion of momentum p_π decays into a muon of kinetic energy T_μ within dT_μ. $P(p_\pi, T_\mu)dT_\mu$ has a very simple form which may be found as follows. In the center of momentum system (primed) the angular distribution of the muons is isotropic.

$$P(\theta')d\theta' = 1/2\ d(\cos\theta') \qquad (11)$$

The Lorentz transformation gives:

$$E_\mu = \gamma(E'_\mu + \beta c p'_\mu \cos\theta')$$

hence

Figure A2. Decay Before the Magnet, Determination of α.

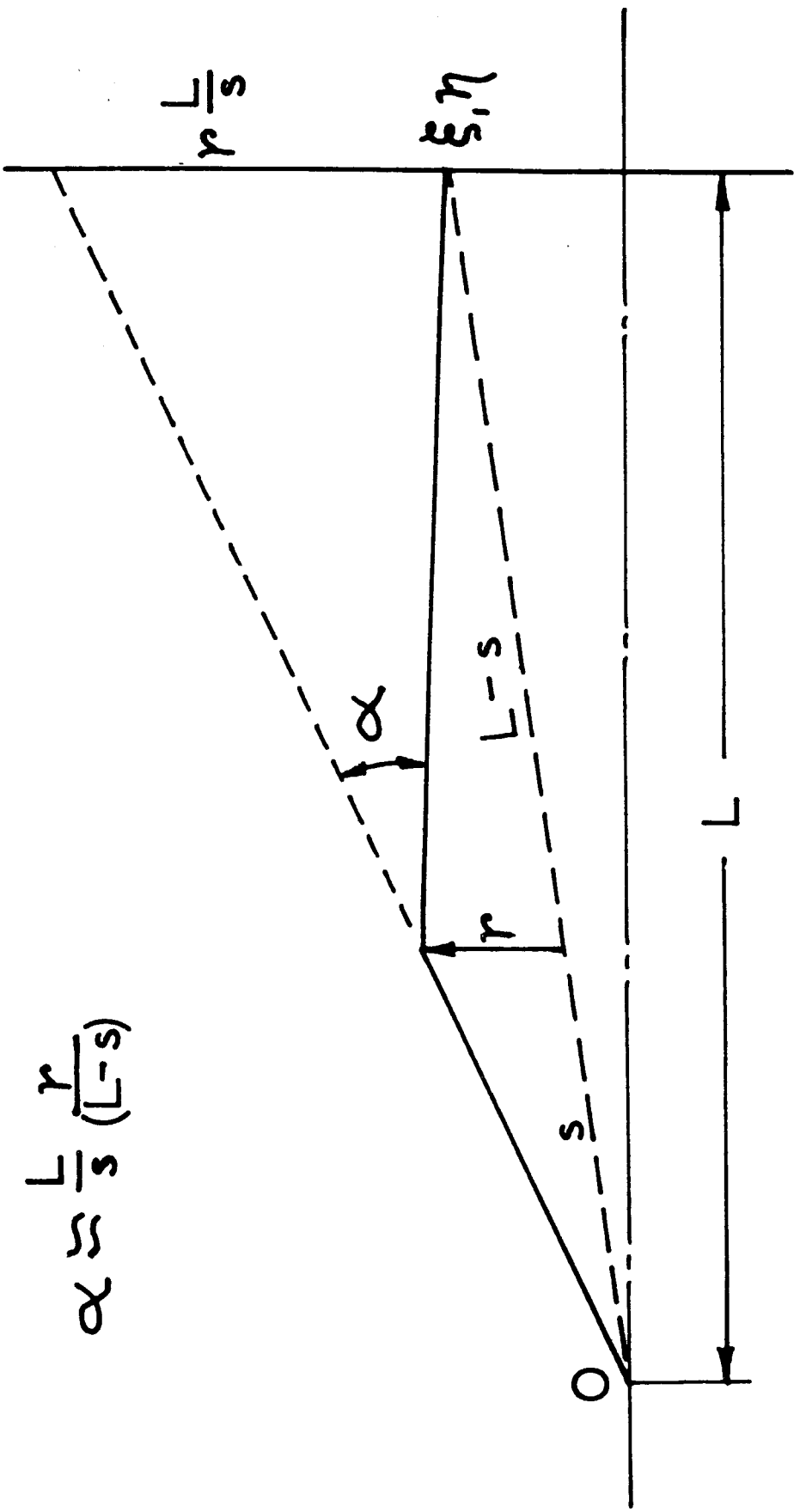
$\frac{L}{s}\xi,\eta$
$\frac{L}{s}r$
α
$L-s$
r
s
L
O
$\alpha \leq \frac{L}{s}\frac{r}{(L-s)}$

$$dE_\mu = dT_\mu = \gamma\beta c\, p'_\mu\, d(\cos\theta') \tag{12}$$

and

$$P(T_\mu)dT_\mu = P(\theta')\, 2\pi d(\cos\theta') = \frac{dT_\mu}{2\gamma\beta c p'_\mu} \tag{13}$$

Now $\gamma\beta c = p_\pi/m$, p'_μ = constant = 29.9 Mev/c. Call $a = m/2p'_\mu$, then:

$$P(p_\pi, T_\mu)dT_\mu = \begin{cases} \dfrac{a dT_\mu}{p_\pi} = \dfrac{a p_\mu dp_\mu}{E_\mu p_\pi} & ; \text{ if } p_{min} < p_\mu < p_{max} \\ \\ 0; \text{ otherwise} \end{cases} \tag{14}$$

Substituting the variable T_μ in place of α into equation 10 we have simply:

$$\gamma(p_\pi, 0) = \frac{1}{\lambda} \int \frac{a p_\mu\, dp_\mu}{\Delta p_o E_\mu p_\pi}$$

and since $p_\mu = p_o$ (within Δp_o) we obtain finally

$$\gamma(p_\pi, 0) = \frac{a p_o}{\lambda p_\pi \sqrt{p_o^2 + m_\mu^2}} = \frac{am p_o}{\tau p_\pi^2 \sqrt{p_o^2 + m_\mu^2}} \tag{15}$$

For a given p_o, $\gamma(p_\pi, 0)$ is then proportional to $1/p_\pi^2$ for $p_{\pi\,min} < p_\pi < p_{\pi\,max}$ and zero elsewhere.

2. Decay at the Entrance Aperture: s = L

Consider an element of surface $d\xi\, d\eta$ of the aperture, centered around the point (ξ, η). The number of pions of momentum p_π which decay in the volume element $d\xi\, d\eta\, ds$ is:

$$Q(p_\pi)dp_\pi \frac{d\xi\, d\eta}{L^2} e^{-L/\lambda} \frac{ds}{\lambda} = e^{-L/\lambda} \frac{ds}{\lambda} Q(p_\pi)dp_\pi d\Omega \qquad (16)$$

The muons which decay at an angle α from the pion trajectories, have for a given p_π two possible values of momentum $p_{\mu 1}$ and $p_{\mu 2}$. The muon rays, when extended in the object space, strike the plane $s = 0$ along a circle centered at the source and having a radius $R = L\alpha$.

We know that the magnification of the spectrometer is unity (symmetric magnet) in the direction perpendicular to the magnetic field. There is no focusing in the direction of the field, but if we choose a small element of surface $d\xi\, d\eta$, there would be an "image" in that direction in the same way that an optical "image" can be obtained with the small opening in a "camera obscura". The "image" of a circle of radius R will then be a circle of same radius but displaced horizontally from the center of the counter by an amount:

$$D = K\,(p_\mu - p_o)/p_o$$

where K is a constant characteristics of the spectrometer (in our case K = 95 cm). The pattern obtained in the counter plane for different values of p_μ is shown in figure A3a.

Figure A3a. Pattern Obtained in the Counter Plane from Muons Originating at one Point of the Entrance Aperture.

Figure A3b. Typical "image" Circles from Muons of a Given Energy Originating at the Entrance Aperture.

a)

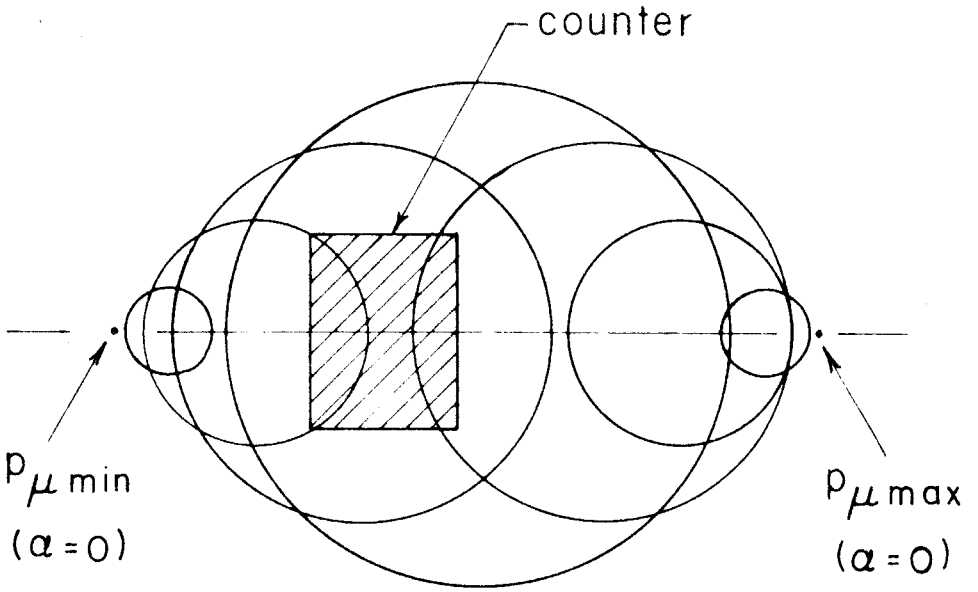
counter
p_μ min
($\alpha = 0$)
p_μ max
($\alpha = 0$)

b)

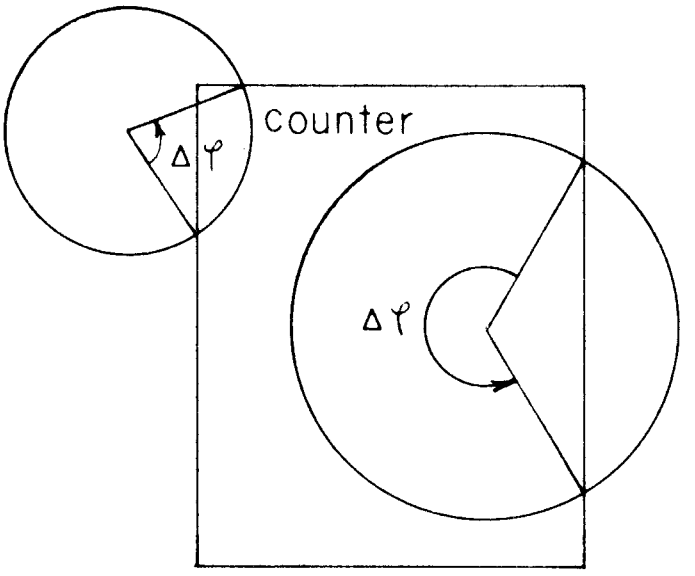
counter
$\Delta\varphi$
$\Delta\varphi$

For a given p_μ (or α), the probability that the muon strikes the counter is given by:

$$P(p_\pi, p_\mu)dp_\mu \Delta\varphi/2\pi = a p_\mu dp_\mu \Delta\varphi/2\pi E_\mu p_\pi \qquad (17)$$

where $\Delta\varphi$ is the arc of the image circle intercepted by the counter (see figure A3b).

The pattern of figure A3a is independent of ξ and it is just displaced vertically for different values of η . Integrating over the aperture is equivalent to take the average of $\Delta\varphi/2\pi$ over the height of the counter. (We make the approximation here that the focused particles are distributed uniformly over the counter height.)

We have now:

$$c_\mu(L)ds = \int_{p_\pi} Q(p_\pi)dp_\pi \Delta\Omega\, e^{-L/\lambda} \frac{ds}{\lambda} \int_{p_\mu} \frac{a p_\mu}{E_\mu p_\pi} \frac{\Delta\varphi_{av}}{2\pi} dp_\mu \qquad (18)$$

and since

$$c_o(L)ds = Q(p_o)\Delta p_o \Delta\Omega\, e^{-L/\lambda_o} ds/\lambda_o \qquad (19)$$

then, from equation 9:

$$\gamma(p_\pi, L) = \frac{am\, e^{-L/\lambda}}{\tau \Delta p_o p_\pi^2} \int_{p_{\mu\min}}^{p_{\mu\max}} \beta_\mu \frac{\Delta\varphi_{av}}{2\pi} dp_\mu \qquad (20)$$

$\Delta\varphi_{av}$ was obtained graphically.

B. Decays Beyond the Magnet

Muons from the decay of pions beyond the magnet will be counted only if the pion is headed nearly at the counters since the decay angles are small. This means that the contribution to the decay correction of the decays beyond the magnet is practically independent of the shape of the pion spectrum $Q(p_\pi)$.

A reasonable approximation of $f(s) = c_\mu(s)/c_o(s)$ will then be simply the probability that the muon from a pion of momentum p_o strikes the counter. The effect of the decay at s of pions which are aimed at a given point is to distribute decay muons in a circle centered at this point and with a radius depending on s and p_μ. As in the previous section the probability that the muon is counted will be obtained by determining an arc $\Delta\varphi$ which should be averaged over the height of the counter for the different allowable values of p_μ (see figure A3b). It should be remembered that, in order for the muon to be able to cross all three counters, its momentum has to be greater tan 95 Mev/c.

We have

$$f(s) = \frac{a}{p_o} \int_{p_{\mu min}}^{p_{\mu max}} \beta_\mu \frac{\Delta\varphi_{av}}{2\pi} \, dp_\mu \qquad (21)$$

and

$$R_{\mu}(\text{beyond magnet}) = \int_{S/2}^{S} f(s)\, e^{-s/\lambda_o}\, \frac{ds}{\lambda_o} \qquad (22)$$

C. Complete Decay Correction

All the decays occurring between s = 0 and s = S/2 are considered "before magnet", those occurring between s = S/2 and S are considered "beyond magnet". Then:

$$g(p_{\pi}) = \int_{o}^{S/2} \gamma(p_{\pi}, s)ds$$

and since we have computed $\gamma(p_{\pi}, s)$ for only two values of s we use a linear interpolation.

$$g(p_{\pi}) \sim \gamma(p_{\pi}, 0)\ \frac{S}{2}\ - \left[\gamma(p_{\pi}, 0) - \gamma(p_{\pi}, L)\right]\ \frac{(S/2)^2}{2L} \qquad (23)$$

The complete decay correction is:

$$R = R_{\pi} + \int \frac{Q(p_{\pi})}{Q(p_o)}\ g(p_{\pi})dp_{\pi} + R_{\mu}(\text{beyond magnet})$$

$$R = R_o + \int q(p_{\pi})\ g(p_{\pi})dp_{\pi} \qquad (24)$$

where $q(p_{\pi}) = \dfrac{Q(p_{\pi})}{Q(p_o)}$ and $R_o = R_{\pi} + R_{\mu}$ (beyond magnet)

We can define the "effective" path length kS for the pions by the relation:

$$R = e^{-kS/\lambda_o} \tag{25}$$

Previous calculations (31) have shown that k is approximately a linear function of the pion energy. We have calculated the decay correction for positive pions produced in a single photoproduction, at two values of pion energies (50 and 125 Mev). The corresponding values of k are plotted in figure A4. A linear interpolation can be used to estimate the π- μ decay correction at other pion energies. It is believed that the values of k plotted in figure A4 give the decay correction within 3 ^{o}/o.

In our experiment, we want to compare the correction at a given p_o for positive pions from single photoproduction to the correction for negative pions which come from a multiple production. Call $q_+(p_\pi)$ and $q_-(p_\pi)$ the corresponding momentum spectra. Then, from equation 24:

$$\frac{R_+}{R_-} = \frac{R_o + \int q_+(p_\pi) g(p_\pi) dp_\pi}{R_o + \int q_-(p_\pi) g(p_\pi) dp_\pi} \tag{26}$$

In general $R_o \gg R_\mu$ (before magnet), hence:

$$\frac{R_+}{R_-} \sim 1 + \frac{1}{R_o} \int_{p_\pi \text{ min}}^{p_\pi \text{ max}} \left[q_+(p_\pi) - q_-(p_\pi) \right] g(p_\pi)\, dp_\pi \tag{27}$$

Figure A4. "Effective Path" Constant k Versus Pion Energy.

The decay correction R is defined by:

$$R = e^{-kS/\lambda_o}$$

where $\lambda_o = \tau p_o/m$

p_o = pion momentum selected by the spectrometer

τ = pion mean life-time

m = pion rest mass.

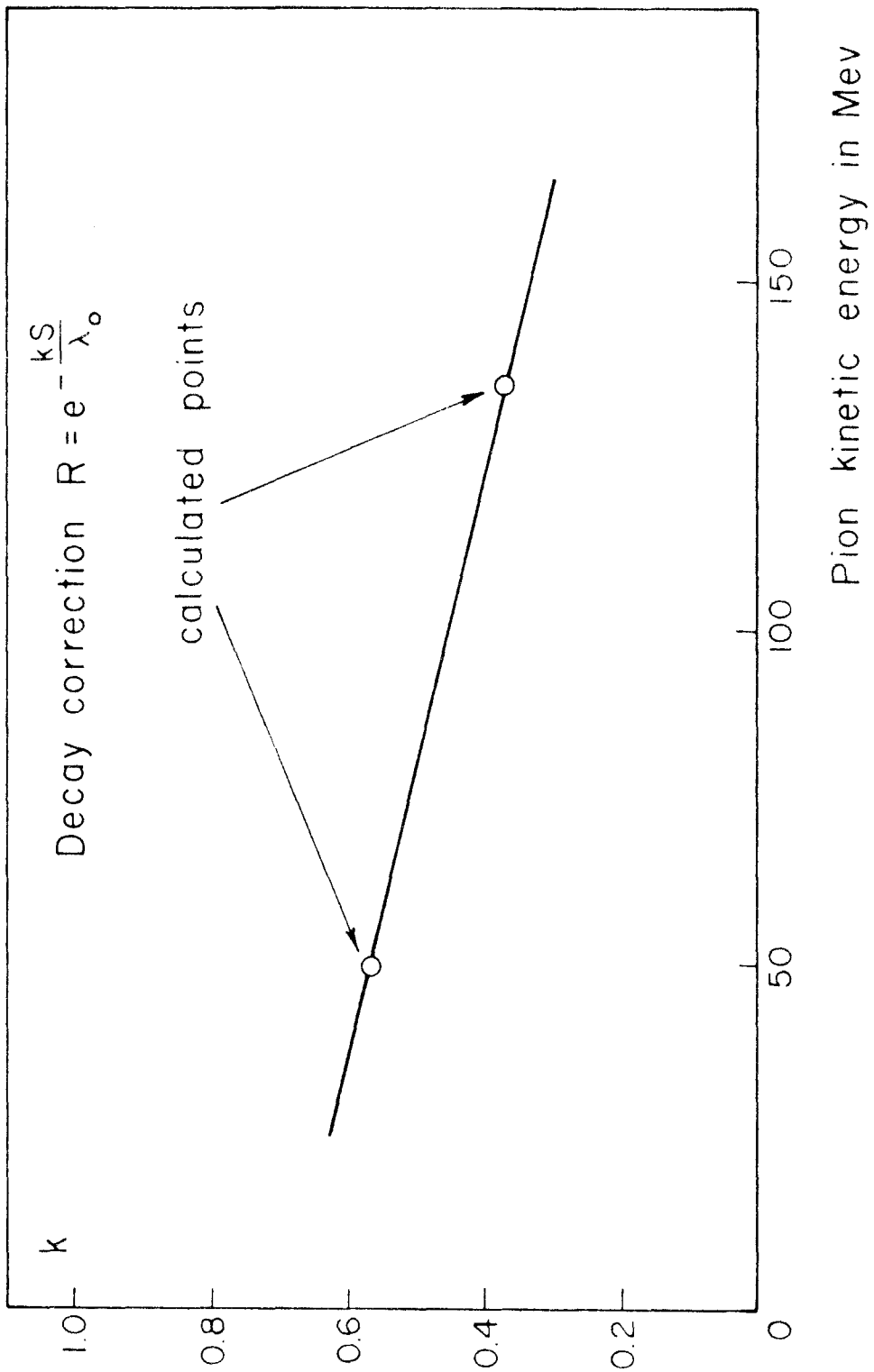
k
1.0
0.8
0.6
0.4
0.2
0
50
100
150
Pion kinetic energy in Mev
Decay correction $R = e^{-\frac{kS}{\lambda_o}}$
calculated points

It turns out that, in the experiment described in this work, $\left[q_+(p_\pi) - q_-(p_\pi)\right]$ stays small in the full range of pion momenta which contribute to the integrals in equation 27. A calculation performed for p_o = 225 Mev/c, the π^- yield being taken at k_{max} = 1.1 Bev, gives the following result:

$$\frac{R_+}{R_-} \sim 1.005$$

The decay correction would also be the same (within 1 $^o/o$) for the two sets of negative pion data which lead to the determination of a cross-section, because the momentum spectrum of negative pions change only slowly with bremsstrahlung cut-off energy.

REFERENCES

1. H. A. Bethe and F. de Hoffmann, Mesons and Fields (Row, Peterson and Company, Evanston 1955) vol. 2 for a summary of much of the literature.

2. G. F. Chew and F. Low, Phys. Rev. 101, 1570, 1579 (1956).

3. V. Z. Peterson and I. G. Henry, Phys. Rev. 96, 850 (1954).

4. M. Sands, M. Bloch, J. Teasdale and R. Walker, Phys. Rev. 99, 652 (1955).

5. V. Z. Peterson, Bull. Am. Phys. Soc. 1, 172 (1956).

6. R. M. Friedman and K. M. Crowe, Phys. Rev. 105, 1369 (1957).

7. R. E. Cutkosky and F. Zachariasen, Phys. Rev. 103, 1108 (1956).

8. W. M. Woodward, R. R. Wilson and P. D. Luckey, Bull Am. Phys. Soc. 2, 195 (1957).

9. M. Bloch and M. Sands, Bull. Am. Phys. Soc. 2, 321 (1957).

10. Eisberg, Fowler, Lea, Shephard, Schutt, Thorndike and Whittemore, Phys. Rev. 97, 797 (1955).

11. W. D. Walker and J. Crussard, Phys. Rev. 98, 1416 (1955).

12. W. D. Walker, F. Hushfar and W. D. Shephard, Phys. Rev. 104, 526 (1956).

13. H. L. Johnston, I. I. Bezman, T. Rubin, C. A. Swanson, W. Corak and E. B. Rifkin, "Low Temperature, High Pressure Data of State for Hydrogen and Deuterium between 64° and 300°K" A.E.C. MDDC-850.

14. The analysis was performed by the Consolidated Electrodynamics Corporation of Pasadena.

15. M. A. Bloch, "Low Energy Spectrometer" unpublished report.

16. P. L. Donoho, unpublished report.

17. R. R. Wilson,preprint.

18. R. Gomez, private communication.

19. P. Donoho, E. Emery and R. Walker, private communication.

20. R. M. Littauer and D. Walker, Phys. Rev. 86, 838 (1952).

21. R. L. Walker, J. G. Teasdale, V. Z. Peterson and J. I. Vette, Phys. Rev. 99, 210 (1955).

22. J. I. Vette, private communication.

23. R. Worlock, private communication.

24. P. L. Donoho, private communication.

25. G. F. Chew, M. L. Goldberger, F. E. Low and Y. Nambu, Phys. Rev. 106, 1345 (1957).

26. S. Berman, private communication.

27. S. J. Lindenbaum and R. M. Sternheimer, Phys. Rev. 105, 1874 (1957).

28. S. J. Lindenbaum and R. M. Sternheimer, Phys. Rev. 106, 1106 (1957).

29. J. E. Crew, R. D. Hill and L. S. Lavatelli, Phys. Rev. 106, 1051 (1957).

30. J. M. Sellen, G. Cocconi, V. T. Cocconi, E. L. Hart and K. C. Rogers, Bull. Am. Phys. Soc. 2, 195 (1957).

31. R. L. Walker and J. I. Vette, unpublished report.